

This is the accepted manuscript made available via CHORUS. The article has been published as:

Majorana surface modes of nodal topological pairings in spin-3/2 semimetals

Wang Yang, Tao Xiang, and Congjun Wu

Phys. Rev. B **96**, 144514 — Published 30 October 2017

DOI: [10.1103/PhysRevB.96.144514](https://doi.org/10.1103/PhysRevB.96.144514)

Majorana surface modes of nodal topological pairings in spin- $\frac{3}{2}$ semi-metals

Wang Yang,¹ Tao Xiang,^{2,3} and Congjun Wu¹

¹*Department of Physics, University of California, San Diego, California 92093, USA*

²*Institute of Physics, Chinese Academy of Sciences, P.O. Box 603, Beijing 100190, China*

³*Collaborative Innovation Center of Quantum Matter, Beijing 100190, China*

When solid state systems possess active orbital-band structures subject to spin-orbit coupling, their multi-component electronic structures are often described in terms of effective large-spin fermion models. Their topological structures of superconductivity are beyond the framework of spin singlet and triplet Cooper pairings for spin- $\frac{1}{2}$ systems. Examples include the half-Heusler compound series of RPtBi, where R stands for a rare-earth element. Their spin-orbit coupled electronic structures are described by the Luttinger-Kohn model with effective spin- $\frac{3}{2}$ fermions and are characterized by band inversion. Recent experiments provide evidence to unconventional superconductivity in the YPtBi material with nodal spin-septet pairing. We systematically study topological pairing structures in spin- $\frac{3}{2}$ systems with the cubic group symmetries and calculate the surface Majorana spectra, which exhibit zero energy flat bands, or, cubic dispersion depending on the specific symmetry of the superconducting gap functions. The signatures of these surface states in the quasi-particle interference patterns of tunneling spectroscopy are studied, which can be tested in future experiments.

I. INTRODUCTION

Topological superconductivity and paired superfluidity have been attracting intense research interests in recent years¹⁻³. The nontrivial topology manifests itself in the Andreev-Majorana zero modes on boundaries and topological defects like vortices⁴⁻⁷. Such Andreev-Majorana modes are of particular interests since they are potentially useful for topological quantum computations⁸⁻¹⁰. Early topological classifications mostly focus on the fully gapped superconducting systems¹¹⁻¹³, including the two-dimensional $p_x + ip_y$ superconductor⁵, and the three-dimensional $^3\text{He-B}$ phase with the isotropic p -wave triplet pairing^{3,14,15}. Recently, gapped topological superconductivity has also been proposed for high T_c cuprates in the very underdoped regime¹⁶.

Gapless, or, nodal, superconductors/pairing superfluids often exhibit unconventional pairing symmetries, such as the d -wave superconductors of high T_c cuprates¹⁷, the three-dimensional $^3\text{He-A}$ phase with the $p_x + ip_y$ triplet pairing^{5,18}, the p_z -triplet pairing phase of electric dipolar fermions¹⁹, and spin-orbit coupled p -wave pairing with total angular momentum $J = 1$ induced by magnetic dipolar interactions²⁰. For these examples, their gap functions exhibit spherical or spin-orbit coupled harmonic symmetries. In contrast, the doped magnetic Weyl semi-metals can support monopole harmonic pairing²¹, which is a class of topological superconducting states characterized by non-trivial monopole structures. Their pairing phases cannot be globally well-defined on Fermi surfaces.

The gapless superconducting systems also exhibit interesting topological structures^{22,23}, which are typically weaker than those in the gapped cases in the sense that only suitably oriented surfaces can support the zero energy Andreev-Majorana states. These surfaces are with particular orientations such that a relative sign change occurs between the gap functions along the incident and

reflected wavevectors. There do not exist well-defined global topological numbers for a gapless system. However, a topological number can be defined for each momentum within the surface Brillouin zone, as the winding number of the effective one-dimensional system perpendicular to the surface with the fixed in-surface momentum. This topological number is related to the existence of zero energy Andreev-Majorana modes through the bulk-edge correspondence principle^{24,25}.

The non-centrosymmetric superconductors add to the diversity of gapless superconductivity²⁴⁻²⁸. In their normal state band structures, the spin degeneracy is lifted by spin-orbit coupling, and pairing gap functions typically show mixed-parity due to the breaking of inversion symmetry. Depending on the pairing symmetry and the nodal structure, there appear Majorana flat bands and zero energy arcs on the surfaces with suitable orientations^{25-27,29}. The experimental signatures include zero-energy peaks in the tunneling spectra^{30,31}, and certain patterns in the quasi-particle interference (QPI)³². The instability of the Majorana flat bands has been studied with respect to the spontaneous time-reversal (TR) symmetry breaking effects arising from the Majorana fermion-superfluid phase interaction³³, or, the magnetic interactions³⁴, and also by the self-consistent mean field theory³⁵.

The superconducting pairing symmetries can be greatly enriched in multi-component fermion/electron systems. In ultra-cold fermion systems, many fermions carry large-hyperfine-spin S larger than $\frac{1}{2}$. In solid state systems, electrons can be effectively multi-component due to orbital degeneracy and spin-orbit splitting, such as the effective spin- $\frac{3}{2}$ Luttinger-Kohn model for the hole band of semi-conductors. The spin of their Cooper pairing can take values from 0 to $2S$ beyond the conventional singlet and triplet scenarios³⁶⁻⁴⁰. For example, the spin quintet pairing (the spin of Cooper pair $S = 2$) has been found to support the non-Abelian Cheshire charge in the

presence of half-quantum vortex loop³⁹. Recently, the ³He-B type isotropic topological pairing has been generalized to multi-component fermion systems⁴⁰. For the simplest case of spin-3/2 systems, both the p -wave triplet and the f -wave septet pairings are non-trivial, possessing topological index 4 and 2, respectively. They support surface spectra with multiple linear and cubic Dirac-Majorana cones^{40,41}. The interaction-induced TR symmetry breaking effects are investigated in Ref. [42]. The topological nature of this class of pairings is most clearly seen in the helicity basis, and thus it also applies to spin-orbit coupled multi-orbital solid state band systems.

Recently, the half-Heusler compound YPtBi has attracted considerable attention^{43,44}. The band structure can be described by the effective spin-orbit coupled spin- $\frac{3}{2}$ Kohn-Luttinger Hamiltonian with parity symmetry breaking terms. The chemical potential lies close to the Γ -point of the p -like Γ_8 band⁴³ as shown in the angular-resolved-photo-emission-spectroscopy. Experiment evidence to unconventional superconductivity has been found in the half-Heusler compound YPtBi⁴⁴. A mixed parity pairing immune to pair breaking effect has been proposed for YPtBi⁴⁵, with a small fraction of an s -wave singlet component superposed on the p -wave septet pairing.

Motivated by the advancements in non-centrosymmetric superconductors, we systematically study the Majorana surface states of topological superconductors based on the spin- $\frac{3}{2}$ Luttinger-Kohn model subject to the cubic symmetries. For the T_d point group symmetry, we show that the double degeneracy along the $[001]$ direction and its equivalent ones are protected by the little group SD_{16} , i.e., the semi-dihedral group of order 16. The pairing patterns in non-centrosymmetric systems are in general of mixed-parity nature as discussed under concrete cubic symmetry groups. For the YPtBi, the proposed mixed s -wave singlet and p -wave septet pairing exhibits line nodes on one of the spin split Fermi surfaces as shown in Ref. [45], and the six nodal loops centering around $[001]$ and its equivalent directions are topological. We show that for the $[111]$ surface, the Majorana zero modes appear in regions enclosed by the projections of the nodal loops to the surface Brillouin zone, but disappear in the overlapping regions. The QPI patterns are calculated on the $[111]$ surface due to the scattering with a single impurity in the Born approximation. For a non-magnetic impurity, the chiral symmetry forbids the scatterings between Majorana islands with the same chiral index, while for a magnetic impurity, the scatterings between Majorana islands with opposite chiral indices are forbidden. The structures of the QPI patterns of a magnetic impurity are richer than those of a non-magnetic impurity under the C_{3v} group, which is the symmetry group of the $[111]$ -surface. Experiments on the QPI patterns will provide tests to the proposed pairing symmetries of YPtBi.

The rest of this article is organized as follows. In Sec.

II, the Luttinger-Kohn Hamiltonian and the band inversion are reviewed. The inversion breaking terms with the cubic symmetries are classified, and the protected double degeneracy of the T_d group along the $[001]$ direction is proved. In Sec. III, the non-centrosymmetric Copper pairings with the cubic symmetries are discussed. The Majorana surface modes are solved in Sec. IV. The QPI patterns are calculated in Sec. V.

II. NON-CENTROSYMMETRIC SPIN- $\frac{3}{2}$ SYSTEMS WITH THE CUBIC SYMMETRIES

In this section, we first discuss the Luttinger-Kohn Hamiltonian in spin-orbit coupled systems, and classify the inversion breaking terms according to the cubic point groups. We then show that for the T_d group, there exists a protected double degeneracy along $[001]$ and its equivalent directions. Finally the band structure properties of the YPtBi material are reviewed.

A. The Luttinger-Kohn Hamiltonian and band inversion

Although electrons carry spin- $\frac{1}{2}$, the effective spin- $\frac{3}{2}$ systems are not rare in solid state materials due to spin-orbit coupling. Examples include the half-Heusler compounds, where spin-orbit coupling recombines the outer-shell s - and p - orbitals into $s_{\frac{1}{2}}$ (Γ_6), $p_{\frac{1}{2}}$ (Γ_7) and $p_{\frac{3}{2}}$ (Γ_8) orbitals, with the subscripts denoting the spin-orbit coupled total angular momentum. The $p_{\frac{1}{2}}$ -band is denoted the “spin-split” band, which is far from the Fermi energy, and will be neglected below. The $s_{\frac{1}{2}}$ and $p_{\frac{3}{2}}$ bands are active, and typically the $s_{\frac{1}{2}}$ band energy is higher. The gap between them is tunable by varying the spin-orbit coupling strength, which can be realized in experiments by substituting the heavy atom with other atomic elements. The gap vanishes at a critical spin-orbit coupling strength, and then becomes negative, i.e., the energy of the $s_{\frac{1}{2}}$ -band becomes lower, which is termed as “band inversion”. The $p_{\frac{3}{2}}$ -band further splits due to spin-orbit coupling according to the helicity quantum number, i.e., the spin projection on the momentum direction. The heavy hole band is of the helicity quantum numbers $\pm\frac{3}{2}$, and the light hole one is of the helicity numbers $\pm\frac{1}{2}$. The heavy and light hole bands touch at the Γ -point, as protected by the cubic group symmetry. All bands are doubly degenerate when TR and inversion symmetries are present.

At the critical spin-orbit coupling strength, where the $s_{\frac{1}{2}}$ - and $p_{\frac{3}{2}}$ -bands touch at the Γ -point, the dispersions of $s_{\frac{1}{2}}$ - and light hole bands become linear, while the heavy hole band remains parabolic. After the band inversion, the curvature of the dispersion of $s_{\frac{1}{2}}$ -band becomes negative, while that of the light hole actually is positive. A

schematic plot of the band structure after band inversion is shown in Fig. 1.

The process of band inversion can be understood by a $k \cdot p$ analysis as follows. Consider systems with the full spin-orbit coupled $SO(3)$ symmetry for simplicity. The $k \cdot p$ basis for $s_{\frac{1}{2}}$ and $p_{\frac{3}{2}}$ -bands are chosen as

$$|s; \uparrow\rangle, |s; \downarrow\rangle, \quad (1)$$

and

$$\begin{aligned} & |p_x + ip_y; \uparrow\rangle, \\ & \frac{1}{\sqrt{3}} \left(|p_x + ip_y; \downarrow\rangle + \sqrt{2}|p_z; \uparrow\rangle \right), \\ & \frac{1}{\sqrt{3}} \left(|-p_x + ip_y; \uparrow\rangle + \sqrt{2}|p_z; \downarrow\rangle \right), \\ & |-p_x + ip_y; \downarrow\rangle, \end{aligned} \quad (2)$$

which are eigen-basis of $S_z = L_z + \frac{1}{2}\sigma_z$ with eigenvalues in a descending order. The three basis at the Γ -point with positive eigenvalues of S_z are $s_{\frac{1}{2}}$, $|p_x + ip_y; \uparrow\rangle$, $\frac{1}{\sqrt{3}}(|p_x + ip_y; \downarrow\rangle + \sqrt{2}|p_z; \uparrow\rangle)$, and the other ones with negative S_z can be obtained from them by the TR operation. Apart from an overall constant the Hamiltonian at the Γ -point in the positive S_z sector is given by

$$H^+(\Gamma) = \begin{pmatrix} m & & \\ & -m & \\ & & -m \end{pmatrix}, \quad (3)$$

in which m is half of the band gap. To obtain the Hamiltonian away from the Γ -point, it is sufficient to consider the z -direction due to the rotation invariance. The little group along this direction is the $U(1)$ group $e^{-iS_z\phi}$, hence, hybridizations only occur between states with the same S_z . The $k \cdot p$ Hamiltonian in the positive S_z sector up to the linear order in k_z is

$$H^+(k_z) = \begin{pmatrix} m & & \lambda k_z \\ & -m & \\ \lambda^* k_z & & -m \end{pmatrix}, \quad (4)$$

in which $m > 0$ and < 0 correspond to before and after band inversion, respectively. The Hamiltonian H^- in the negative S_z sector can be obtained by applying the TR operation to Eq. (4). The $k \cdot p$ Hamiltonian in the basis of Eqs. (1, 2) along a general direction of \vec{k} can be constructed by performing the rotation operation $U = e^{-iS_z\phi_k} e^{-iS_y\theta_k}$ on $H^+(k_z) + H^-(k_z)$ where θ_k and ϕ_k are the polar and azimuthal angles of \vec{k} , respectively. At the critical point $m = 0$, the $s_{\frac{1}{2}}$ - and light hole band dispersions become linear with the velocity $\pm \frac{|\lambda|}{\hbar}$.

Consider the case with band inversion as illustrated in Fig. 1, where the Fermi energy lies close to the Γ -point of the $p_{\frac{3}{2}}$ -bands. Only the $p_{\frac{3}{2}}$ -bands are taken into account with the $k \cdot p$ basis chosen as the four states in Eq. (2), and the band structure is captured by the

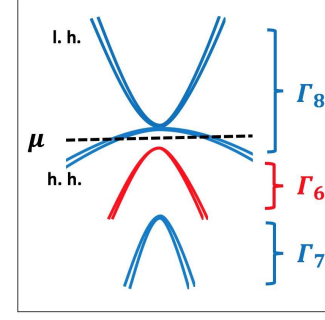


FIG. 1: Schematic plots of the $p_{\frac{3}{2}}$ - bands (Γ_8), $p_{\frac{1}{2}}$ - bands (Γ_7), and $s_{\frac{1}{2}}$ - bands (Γ_6). The abbreviations of “h. h.” and “l. h.” within the $p_{\frac{3}{2}}$ -bands represent the heavy and light hole bands, respectively. The Fermi level crosses the heavy hole bands. Each pair of bands exhibit spin splitting due to the presence of the inversion symmetry breaking term $\frac{\delta}{k_f} A(\vec{k})$ in Eq. (6).

Luttinger-Kohn Hamiltonian

$$\begin{aligned} H_L(\vec{k}) = & (\lambda_1 + \frac{5}{2}\lambda_2)k^2 - 2\lambda_2(\vec{k} \cdot \vec{S})^2 \\ & + \lambda_3 \sum_{i \neq j} k_i k_j S_i S_j, \end{aligned} \quad (5)$$

in which $\vec{S} = (S_x, S_y, S_z)$ are the spin- $\frac{3}{2}$ operators. The λ_3 term breaks the full spin-orbit coupled $SO(3)$ rotational symmetry, but is allowed for the cubic symmetry group. When $\lambda_3 = 0$, the mass of helicity $\pm \frac{3}{2}$ bands is $\frac{\hbar^2}{2(\lambda_1 - 2\lambda_2)}$, and that of the helicity $\pm \frac{1}{2}$ bands is $\frac{\hbar^2}{2(\lambda_1 + 2\lambda_2)}$. For the band inverted case, we need $-2\lambda_2 < \lambda_1 < 2\lambda_2$ to ensure the opposite signs of the light and heavy hole masses.

B. Non-centrosymmetric spin-orbit couplings with the cubic symmetries

We classify all the TR and cubic symmetry allowed $k \cdot p$ terms up to the quadratic order in k . The Hamiltonian Eq. (5) includes all the inversion invariant terms up to the k^2 -part from an overall constant. Inversion breaking terms are allowed for the three cubic groups O, T_d, T . The corresponding band Hamiltonian becomes

$$H_0(\vec{k}) = H_L(\vec{k}) + \frac{\delta}{k_f} A(\vec{k}), \quad (6)$$

in which $A(\vec{k}) = -A(-\vec{k})$ breaks inversion symmetry, k_f is the Fermi wave vector, and δ parameterizes the inversion breaking strength. To the lowest order in momen-

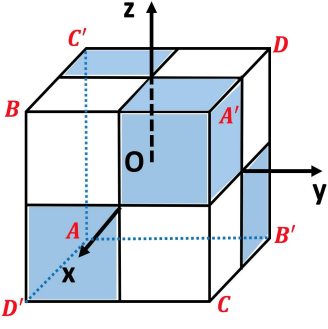


FIG. 2: The decorated cube with the T_d symmetry.

tum, the TR invariant $A(\vec{k})$ takes the form

$$\begin{aligned} T_d : & k_i \cdot (S_{i+1}S_iS_{i+1} - S_{i+2}S_iS_{i+2}), \\ O : & k_i \cdot S_i + a_1 k_i \cdot S_i^3, \\ T : & k_i \cdot S_i + b_1 k_i \cdot S_i^3 + b_2 k_i \cdot (S_{i+1}S_iS_{i+1} \\ & - S_{i+2}S_iS_{i+2}), \end{aligned} \quad (7)$$

in which a_1, b_1, b_2 are numerical factors, and the indices $i, i+1$ are defined cyclicly for x, y, z and the summation over i is assumed. Detailed discussions are included in Appendix A.

C. Protected degeneracy along the $[001]$ direction with the T_d symmetry

The band structure of Eq. (6) does not exhibit double degeneracy in general due to the breaking of inversion symmetry. Interestingly, for the T_d group, there is a protected non-Kramers degeneracy along $[001]$ and its equivalent directions explained as follows.

The illustration of the T_d symmetry in terms of a decorated cube is shown in Fig. 2. Its little group along the $[001]$ direction contains two mirror reflections along the diagonal directions $y = \pm x$ denoted as x' and y' , respectively. The corresponding operations are denoted as $M_{x'}$ and $M_{y'}$, respectively. Since $M_{x'}M_{y'} = R(\hat{z}, \pi)$, where $R(\hat{n}, \phi)$ denotes the rotation around the \hat{n} axis at the angle of ϕ , the little group L_0 of T_d along the $[001]$ direction is

$$L_0 = \{\mathbb{1}, M_{x'}, M_{y'}, R(\hat{z}, \pi)\}, \quad (8)$$

which is isomorphic to the dihedral group D_2 . In half-odd integer spin representations, the 2π -rotation equals -1 , and hence L_0 is doubled as

$$\begin{aligned} L_1 = \{ & \mathbb{1}, M_{x'}, M_{y'}, R(\hat{z}, \pi), \\ & \bar{\mathbb{1}}, \bar{\mathbb{1}}M_{x'}, \bar{\mathbb{1}}M_{y'}, \bar{\mathbb{1}}R(\hat{z}, \pi)\}, \end{aligned} \quad (9)$$

in which $\bar{\mathbb{1}}$ denotes the 2π -rotation. As discussed in Appendix B, L_1 is in fact isomorphic to the quaternion group Q_8 . Different from D_2 , Q_8 is non-Abelian, and

has four 1D irreducible representations and one 2D irreducible representation. The half-odd integer spin representations do not contain the 1D representation of Q_8 shown as follows:

$$M_{x'}M_{y'} = -M_{y'}M_{x'} \quad (10)$$

for half-odd integer spins, since $(M_{x'}M_{y'})^2 = R^2(\hat{z}, \pi) = \bar{\mathbb{1}}$. This anti-commutativity protects the double degeneracy along the $[001]$ direction.

There is another mechanism of the degeneracy protection based on an anti-unitary symmetry \mathcal{S} . It is constructed based on the T_d group and the TR operation \mathcal{T} as

$$\mathcal{S} = R(\hat{z}, \frac{\pi}{2})\mathcal{I} \cdot \mathcal{T} \quad (11)$$

where \mathcal{I} is the inversion operator which flips the momentum direction and acts as the identity operator in spin space, and T is the Kramers TR operation satisfying $\mathcal{T}^2 = -1$. \mathcal{S} leaves the $[001]$ -direction invariant. It is easy to verify that \mathcal{S} 's quartic power is -1 , i.e.,

$$\mathcal{S}^4 = -1. \quad (12)$$

Nevertheless, unlike the Kramers operation, $\mathcal{S}^2 = -R(\hat{z}, \pi)$ which remains an operator instead of a constant. Still \mathcal{S} ensures the double degeneracy of electron states with $\vec{k} \parallel \hat{z}$ ⁴⁶, which can be proved by contradiction. If there was no degeneracy, each Bloch wave state $|\psi_k\rangle$ must be a simultaneous eigenstate of both the Hamiltonian and the operator \mathcal{S} , then $\mathcal{S}|\psi\rangle = \lambda|\psi\rangle$, where λ is a complex number of unit norm. This implies that $\mathcal{S}^2|\psi\rangle = |\lambda|^2|\psi\rangle$ due to the anti-unitarity of \mathcal{S} , and then $\mathcal{S}^4|\psi\rangle = |\psi\rangle$ which is in contradiction with the property $\mathcal{S}^4 = -1$.

Including the anti-unitary operation \mathcal{S} , the little group along the $[001]$ direction is extended from the double group L_1 to SD_{16} , the semi-dihedral group of order 16. Detailed discussions about SD_{16} are included in Appendix B.

Both degeneracy protection mechanisms are general beyond the $k \cdot p$ approximation. The degeneracy is held for any band Hamiltonian with the T_d and TR symmetries realized by half-integer fermions. It even applies to the Bogoliubov excitation spectra in the superconducting states which maintain these symmetries.

D. The YPtBi material

We briefly review the YPtBi material and its band structure. It is an half-Heusler compound with band inversion. The active atomic orbitals are the $6s$ and $6p$ orbitals from the Bi atom. The Pt and Bi atoms form a zinc-blende sublattice, and the Y atoms fill in the lattice such that the Pt and Y atoms form another zinc-blende sublattice^{47–49}. The system has the TR and T_d point group symmetries, but is not inversion symmetric.

The charge carrier density of YPtBi is very low around $2 \times 10^{18} \text{cm}^{-3}$ as revealed by the Shubnikov-de Hass (SdH) oscillation experiments⁴⁴. The corresponding Fermi energy is on the order of $10^2 K$ with the Fermi wave vector one order smaller than the Brillouin zone boundary, such that the $k \cdot p$ description around the Γ -point is applicable. The $k \cdot p$ Hamiltonian $H_0(\vec{k})$ of effective spin- $\frac{3}{2}$ particles has been proposed for YPtBi⁴⁵ as a combination of the Luttinger-Kohn Hamiltonian in Eq. (5) and an inversion breaking term given corresponding to the T_d group in Eq. (7). The inversion breaking term breaks the double degeneracy except along $[001]$ directions, and leads to the spin-split Fermi surfaces with the energy splitting on the order of $10K$. The distortion of the Fermi surfaces away from the perfect sphere induced by the λ_3 -term in Eq. (5) is shown to be a small effect as revealed by the SdH oscillation experiments⁴⁴, which will be neglected in later calculations.

III. NON-CENTROSYMMETRIC SPIN- $\frac{3}{2}$ COOPER PAIRINGS

In this section, we first discuss the non-centrosymmetric Cooper pairings under cubic group symmetries. Then the possible pairing symmetries of YPtBi are briefly reviewed.

A. Non-centrosymmetric Cooper pairings with cubic symmetries

We discuss the Cooper pairings in non-centrosymmetric systems with the TR and cubic group symmetries, which can be viewed as analogues of the $^3\text{He-B}$ pairing in the lattice. The generalization of the $^3\text{He-B}$ pairing to the large spin and high partial-wave channels in continuum has been studied in Ref. [40].

The Bogoliubov-de Gennes (B-deG) Hamiltonian of a spin- $\frac{3}{2}$ superconductor is

$$H_{\text{B-deG}} = \sum_{\vec{k}} (c^\dagger(\vec{k}), c(-\vec{k})^T) H(\vec{k}) \begin{pmatrix} c(\vec{k}) \\ c^\dagger(-\vec{k}) \end{pmatrix}, \quad (13)$$

in which $\sum_{\vec{k}}$ denotes summing over half of momentum space, and $c(\vec{k}) = (c_{3/2}(\vec{k}), c_{1/2}(\vec{k}), c_{-1/2}(\vec{k}), c_{-3/2}(\vec{k}))^T$. The matrix kernel $H(\vec{k})$ is represented as

$$H(\vec{k}) = \begin{pmatrix} H_0(\vec{k}) - \mu & \Delta(\vec{k}) \\ \Delta^\dagger(\vec{k}) & -(H_0(-\vec{k}) - \mu)^T \end{pmatrix}, \quad (14)$$

in which $H_0(\vec{k})$ is the band structure given by Eq. (6), and μ is the chemical potential measured from the Γ point of the $p_{3/2}$ -bands. The pairing term $\Delta(\vec{k})$ is given as

$$\Delta(\vec{k}) = K(\vec{k})R, \quad (15)$$

in which $K(\vec{k})$ denotes the pairing kernel, and R is the charge conjugation matrix defined as $R_{\alpha\beta} = (-)^{\alpha+\frac{1}{2}}\delta_{\alpha,-\beta}$ with α spin indices³⁸. For non-centrosymmetric systems, the breaking of the inversion symmetry mixes pairings with different parities. The pairing kernel $K(\vec{k})$ has been proposed to take the form⁵⁰

$$K(\vec{k}) = \Delta_s + \frac{\Delta_p}{k_f} A(\vec{k}), \quad (16)$$

in which $A(\vec{k})$ is given by Eq. (7) for the cubic groups O, T_d, T ; Δ_s and Δ_p parameterize the strength of the s and p -wave components, respectively. Such pairing avoids the pair breaking effect induced by the inversion breaking term $\frac{\delta}{k_f} A(\vec{k})$ in the band structure⁵⁰, and thus is conceivably to be energetically favorable. The pairing only takes place between electrons from the same spin-split Fermi surface. Nevertheless, we would like to emphasize that the actual superconducting gap symmetry of the YPtBi material is still undetermined, and this is only one possibility that needs to be tested in future experiments.

B. The superconducting properties of the YPtBi material

In this part we give a brief review to the superconducting properties of the YPtBi material, particularly its topological nodal line structure in the gap function. Its transition temperature is $T_c = 0.78K$. Its London penetration depth exhibits a linear temperature dependence⁴⁴, which is a strong evidence for a gap function with nodal lines.

Let us first consider the band eigenstates of H_0 defined in Eq. (6) with A defined as

$$A(\vec{k}) = \sum_{i=x,y,z} k_i (S_{i+1} S_i S_{i+1} - S_{i+2} S_i S_{i+2}), \quad (17)$$

which maintains the TR and T_d symmetries. At $|\delta| \ll |\mu|$, the main effect of the inversion symmetry breaking term is within the heavy hole band and the light hole one to split the double degeneracy. The mixing between heavy and light hole bands is small and will be neglected. Since the Fermi surface cuts the heavy hole band, we project the 4×4 matrix kernel $A(\vec{k})$ into the heavy hole bands. Then $A(\vec{k})$ becomes a 2×2 matrix $\vec{\Lambda}(\vec{k}) \cdot \vec{\tau}$ where $\vec{\tau}$ is the Pauli matrices under the basis with helicities $\pm \frac{3}{2}$, and

$$\begin{aligned} \Lambda_x(\vec{k}) &= -\frac{9k}{8} \sin 2\theta_k \cos 2\phi_k, \\ \Lambda_y(\vec{k}) &= \frac{9k}{16} (3 + \cos 2\theta_k) \sin \theta_k \sin 2\phi_k, \\ \Lambda_z(\vec{k}) &= 0, \end{aligned} \quad (18)$$

with θ_k and ϕ_k the polar and azimuthal angles of \vec{k} , respectively. Then the heavy hole energies exhibit the split-

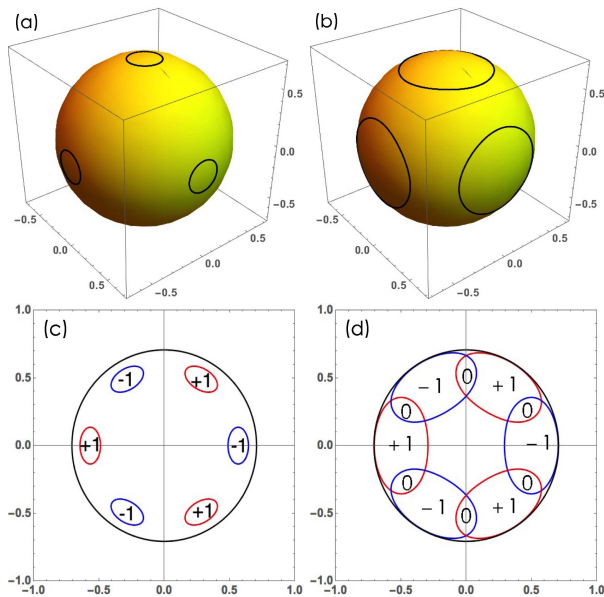


FIG. 3: Nodal loops of the superconducting gap function on the larger spin-split Fermi surface for *a*) $\Delta_s/\Delta_p = 0.3$ and *b*) $\Delta_s/\Delta_p = 0.7$, and projections of the nodal loops to the (111) -surface for *c*) $\Delta_s/\Delta_p = 0.3$ and *d*) $\Delta_s/\Delta_p = 0.7$. In (*c*) the topological numbers are +1 and -1 in the regions enclosed by the red loops and the blue loops, respectively, and are zero outside the loops. In (*d*) the situation is similar except that the topological numbers are zero in the overlapping regions of the loops. The three axes in *a*), *b*) and the two axes in *c*), *d*) are momenta in the bulk Brillouin zone and surface Brillouin zone, respectively, in which the momenta are measured in the unit of $\sqrt{2}k_f$. The Luttinger parameters are taken as $\lambda_1 = 0$ and $\lambda_2 = |\mu|/(2k_f^2)$.

ting of $\delta/k_f|\Lambda(\vec{k})|$ which becomes zero along the $[001]$ and its equivalent directions.

It has been proposed for YPtBi that its pairing symmetry is likely of the mixed *s*-wave singlet and *p*-wave septet⁴⁵. The B-deG Hamiltonian is given by Eq. (14), which maintains the TR and T_d symmetries. The Bogoliubov quasi-particle spectrum exhibits line nodes centering around $[001]$ directions when $\Delta_s/\Delta_p \neq 0$ ⁴⁵. Based on a similar basis as above, when projected into the two spin-split Fermi surfaces belonging to the heavy holes, the diagonalized gap functions becomes $\Delta_s \pm \Delta_p|\vec{\Lambda}(\vec{k})|$. Hence, the gap function becomes nodal on one of the spin-split Fermi surfaces at $|\vec{\Lambda}(\vec{k})| = \Delta_s/\Delta_p$, and the node lines form closed loops centering around $[001]$ and its equivalent directions. The plots of the nodal loops on the corresponding Fermi surface are shown in Fig. 3 (*a,b*) for two representative ratios between Δ_s and Δ_p , for which the nodal loops do not cross, or, cross, respectively.

The nodal loops centering around $[001]$ and its equivalent directions are topologically non-trivial^{24,44}. An integer-valued index can be assigned to each nodal loop as the topological number of a closed loop in momentum space linked with the nodal one on the Fermi surface²⁴.

For a non-trivial nodal loop, the gap functions located inside and outside the nodal loop on the Fermi surface are with opposite signs. Now consider a 2D surface and the associated surface Brillouin zone, the projection of the nodal loop in the 2D Brillouin zone becomes a 2D planar loop. For each momentum in the surface Brillouin zone, it represents an effective 1D system perpendicular to the surface. Hence, a topological number can be defined for each 2D surface momentum except that on the nodes²⁴. The gap functions of the incident wave and the reflection wave perpendicular to the surface change sign if their common 2D momentum is inside the planar projection loop. Hence, for the surface states, their topological numbers are non-trivial for those inside the 2D projection loop but trivial for those outside. But for those in the overlapping regions between two projection loops, they become trivial again. The schematic plot for the case of the $[111]$ -surface is taken as an example for illustration, as shown in Fig. 3 (*c, d*) for two representative ratios between Δ_s and Δ_p . Detailed discussions of the topological properties of the nodal loops are included in Appendix D.

IV. MAJORANA SURFACE STATES

In this section, we first derive the equation solving the Majorana surface states for the spin- $\frac{3}{2}$ systems. The corresponding calculations were performed for the fully gapped isotropic *p*-wave triplet and *f*-wave septet for the continuum model before⁴⁰. Here we consider the gapless mixed parity pairing state explained in the last section. For simplicity, we set $\lambda_3 = 0$ in the band Hamiltonian, and consider the limit of $\Delta_s, \Delta_p \ll \delta \ll |\mu|$. This limit is justified in YPtBi, since $\Delta_s, \Delta_p \sim 1K$, $\delta \sim 10K$, and $\mu \sim 10^2K$. The equation is then applied to obtain the Majorana surface modes for systems with TR and T_d symmetries and also for those with the *T*, or, *O* symmetry.

A. The methodology

Consider a surface with the normal direction along $\hat{n} = (\sin\theta_n \cos\phi_n, \sin\theta_n \sin\phi_n, \cos\theta_n)$. To simplify calculations, we rotate \hat{n} into the *z*-axis. The bulk of the system lies at $z < 0$, and the side of $z > 0$ is vacuum. The boundary condition is that the wavefunction vanishes at $z = 0$ and exponentially decays to zero when $z \rightarrow -\infty$. Within the rotated coordinates, the Luttinger Hamiltonian, the inversion breaking term in band structure, and

the pairing Hamiltonian are expressed as follows,

$$\begin{aligned}
 H_L(-i\vec{\nabla}) &= -(\lambda_1 + \frac{5}{2}\lambda_2)\nabla^2 - 2\lambda_2 \left(R_n(-i\vec{\nabla}) \cdot \vec{S} \right)^2 \\
 &\quad - \mu, \\
 H_A(-i\vec{\nabla}) &= \frac{\delta}{k_f} A \left(R_n(-i\vec{\nabla}) \right), \\
 \Delta(-i\vec{\nabla}) &= K \left(R_n(-i\vec{\nabla}) \right) R,
 \end{aligned} \tag{19}$$

where $R_n = R(\hat{z}, \phi_n)R(\hat{y}, \theta_n)$ is the rotation operation transforming \hat{z} to \hat{n} , $R_n(-i\vec{\nabla})$ represents the rotation of the vector operator $-i\vec{\nabla}$, i.e.,

$$R_{n,a}(-i\vec{\nabla}) = -iR_{n,ab}\nabla_b, \tag{20}$$

where $a = x, y, z$, and $R_{n,ab}$ is the 3×3 rotation matrix. The momenta k_x and k_y parallel to the surface plane remain conserved.

We use the trial plane wavefunction as

$$\Psi(\vec{r}) = \sum_l C_l \Phi_l e^{i\vec{k}_l \cdot \vec{r}}, \tag{21}$$

where Φ_l is an eight-dimensional column vector with four spin components of both particle and hole degrees of freedom. Plug Eq. (21) into the eigen-equation, we obtain

$$\begin{pmatrix} H_0(R_a \vec{k}_l) - \mu & \Delta(R_a \vec{k}_l) \\ \Delta^\dagger(R_a \vec{k}_l) & -(H_0(-R_a \vec{k}_l) - \mu)^T \end{pmatrix} \Phi_l = E_s \Phi_l, \tag{22}$$

where $\vec{k}_l = (k_x, k_y, k_z)$, and E_s is the surface state energy. The boundary condition requires that $\text{Im}k_{zl} < 0$, and there are eight solutions of k_{zl} satisfying this condition, i.e., $1 \leq l \leq 8$: Four come from the sector of helicity eigenvalues $\pm \frac{3}{2}$ and the other four from helicity eigenvalues $\pm \frac{1}{2}$. Furthermore, the boundary conditions require that

$$\sum_{l=1}^8 C_l \Phi_l = 0. \tag{23}$$

In order to have non-trivial solutions of C_l , the determinant composed of the eight column vectors needs to be zero, i.e.,

$$\det \left(\{ \Phi_l \}_{1 \leq l \leq 8} \right) = 0, \tag{24}$$

which determines the surface state eigen-energies. The explicit forms of the eight column vectors Φ_l 's in the limit of $\Delta_s, \Delta_p \ll \delta \ll |\mu|$ are derived in Appendix E.

B. Majorana zero modes under the T_d symmetry

In this part, we solve for the zero energy Majorana surface modes. Let us consider the (001), and (110)-surfaces. From the gap nodal loop configurations shown

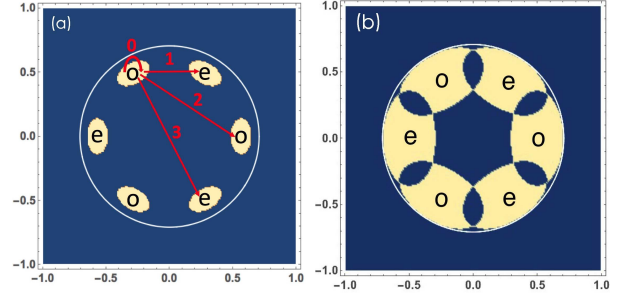


FIG. 4: Distribution of Majorana zero modes in the surface Brillouin zone in the (111)-surface for a) $\Delta_s/\Delta_p = 0.3$ and b) $\Delta_s/\Delta_p = 0.7$. The white circle denotes the boundary of the projection of the Fermi surface. Majorana zero modes exist in the bright regions. The chiral index is marked for each island of the Majorana flat band, where “e” and “o” represent “even” and “odd” with the chiral eigenvalue ± 1 , respectively. The horizontal and vertical axes are momenta in the surface Brillouin zone measured in the unit of $\sqrt{2}k_f$. The Luttinger parameters are taken as $\lambda_1 = 0$ and $\lambda_2 = |\mu|/(2k_f^2)$. The numerical computations are carried out for a 200×200 lattice in momentum space.

in Fig. 3, the nodal loop projections fully overlap with each other, such that all the momentum-dependent topological numbers are trivial. Hence we will only consider the (111)-surface. Through out the calculations the Luttinger parameters are taken as $\lambda_1 = 0$, $\lambda_2 = |\mu|/(2k_f^2)$ and $\lambda_3 = 0$.

The results of Majorana spectra on the (111)-surface are presented in Fig. 4. Fig. 4 (a) shows the case that the projections of the gap nodal loops do not overlap, and the surface zero Majorana modes appear inside the projection loops. In Fig. 4 (b), the projections overlap, and the zero Majorana modes in the overlap region disappear. The former corresponds to a smaller value of $\Delta_s/\Delta_p = 0.3$, and the latter is with a larger one $\Delta_s/\Delta_p = 0.7$. Since each non-trivial momentum dependent topological index equals either 1 or -1 as shown in Fig. 3, these surface zero Majorana modes are non-degenerate. The surface spectra solved from matching boundary conditions are consistent with the previous analysis based on bulk topological number. This can be seen as a verification of the bulk-edge correspondence principle in the spin-3/2 situation.

We then analyze the symmetry properties of the Majorana surface states. Based on the T_d and the TR symmetry, the symmetry subgroup for the (111)-surface is $C_{3v} \times \{1, \mathcal{T}\}$, where \mathcal{T} is the TR operation defined as $\mathcal{T}c^\dagger(\vec{k})\mathcal{T}^{-1} = c^\dagger(\vec{k})R \cdot K$, with K the complex conjugate operation. The surface spectra in Fig. 4 exhibit the C_{3v} -symmetry. The TR operation reverses the momentum direction, and the spectra are also invariant under the TR operation. Consider the particle-hole operation P_H defined as $P_H c_\alpha^\dagger(\vec{k}) P_H^{-1} = c_\alpha(\vec{k})K$. P_H anti-commutes with B-deG Hamiltonian Eq. (14) and transforms a state to another state with the opposite energy. Since Majorana

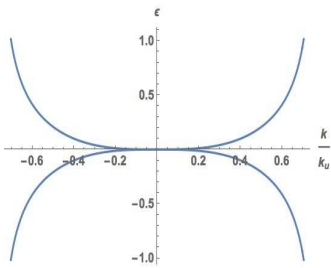


FIG. 5: Surface spectrum of p -wave triplet pairing along radial direction. The horizontal axis is the momentum measured in the unit of $k_u = \sqrt{2}k_f$, and vertical axis is the surface energy measured in the unit of Δ_p .

surface modes are at zero energy, they are particle-hole symmetric.

We can also define a chiral operator as

$$C_{ch} = i\mathcal{T}P_H. \quad (25)$$

It is Hermitian in half-odd integer spin spaces: $C_{ch}^\dagger = -iP_H^\dagger\mathcal{T}^\dagger = C_{ch}$, since $\mathcal{T}^\dagger = \mathcal{T}^{-1} = -\mathcal{T}$ (as $\mathcal{T}^2 = -1$), $P_H^\dagger = P_H$, and $[\mathcal{T}, P_H] = 0$. Both TR and particle-hole operations reverse the sign of the momentum, hence, C_{ch} maintains momentum invariant. This implies that each Majorana zero mode solved above can be chosen as a chiral eigen-state with a chiral index of ± 1 . Since C_{ch} commutes with the C_{3v} group, the islands related by the C_{3v} group carry the same chiral index. While the two islands related by TR operation carry opposite chiral indices, because C_{ch} anti-commutes with the TR operator.

C. The T and O groups

In this part we briefly present the surface spectra calculation of the p -wave triplet pairing for point groups O and T . While the situation of the p -wave triplet pairing with band inversion and the Fermi energy tuned to cross the heavy hole bands has been sketched based on physical intuitions⁴¹, here, we perform a detailed calculation. The band structure and the Cooper pairing are given by Eq. (6) and Eq. (15), respectively, in which $A(\vec{k})$ takes the corresponding form for O and T groups in Eq. (7). Here we consider the p -wave triplet dominant pairing, i.e., $A(\vec{k}) = k_i \cdot S_i$. Unlike the case of p -wave septet pairing under the T_d symmetry, the p -wave triplet pairing under the T and O point groups is $SO(3)$ invariant under the combined orbital and spin rotations. Hence, the quasi-particle spectrum is fully gapped on the Fermi surface. For small enough parameters a_1, b_1, b_2 in Eq. 7 and the ratio Δ_s/Δ_p in Eq. (16), they can be set to zero without affecting topological properties since the pairing is fully gapped. In this case, the B-deG Hamiltonians for the T and O point group symmetries are the same. The system belongs to the $DIII$ class due to the TR and

particle-hole symmetries. The bulk topological number is 3 as a sum of those from the helicity $\pm\frac{3}{2}$ bands⁴⁰. Fig. 5 shows the surface spectrum along the radial direction in the polar coordinate within the surface Brillouin zone. The full spectrum can be obtained by performing a rotation around the normal direction. The overall surface spectrum exhibit the cubic Dirac dispersions^{40,41}, which is consistent with the bulk topological number.

V. QUASI-PARTICLE INTERFERENCE PATTERNS

The scanning tunneling spectroscopy measures the local density of states (LDOS) on the sample surface. In the presence of an impurity, the LDOS exhibits interference pattern due to the scattering of electrons by impurities. The quasi-particle interference (QPI) patterns provide information to the pairing symmetry of high- T_c superconductors⁵¹, orbital ordering in 2D materials⁵², surface states of topological insulators⁵³ and semi-metals⁵⁴. The QPI patterns have also been discussed for various spin-1/2 non-centrosymmetric superconductors³².

In this section, we use the wavefunctions of the surface states solved from Sec. IV B to compute the QPI patterns of a single impurity on the surface of the spin- $\frac{3}{2}$ topological superconductor with the TR and T_d symmetries. Experiments on QPI patterns provide test to the proposed pairing form in Eq. (16).

A. Spin-resolved local density of states

The impurity can be either magnetic or non-magnetic, and the tunneling spectroscopy can be either spin-resolved or non-spin-resolved. In consideration of these, the LDOS tensor $\rho^{\mu\nu}$ is defined with $\mu, \nu = 0, 1, 2, 3, 4$, whose (μ, ν) element is the spin-resolved LDOS for spin in μ -direction with impurity spin polarized in ν -direction. The cases of $\mu = 0$ and $\nu = 0$ correspond to non-spin-resolved and non-magnetic impurity, respectively. To facilitate the symmetry analysis, we rotate the coordinate frame to $\hat{x}' = \frac{1}{\sqrt{6}}(1, 1, -2)$, $\hat{y}' = \frac{1}{\sqrt{2}}(-1, 1, 0)$, $\hat{z}' = \frac{1}{\sqrt{3}}(1, 1, 1)$. The little group of T_d along the (111) -direction is C_{3v} . The three-fold rotation axis in C_{3v} is the \hat{z}' -axis, and the three vertical reflection planes are the $x'z'$ -plane and the $\pm\frac{2\pi}{3}$ rotations of the $x'z'$ -plane around z' -axis. To simply notation, below we still use x, y, z to represent x', y' and z' , i.e., to suppress the $'$ symbol, and use the Greek index $\nu = 1, 2, 3$ to represent them, respectively.

Let us comment on the modeling of the impurity potential in calculations below. For simplicity, the non-magnetic impurity potential V_{imp} is used as an example, which can be straightforwardly extended to the magnetic impurity potential. Typically, it is taken a short range δ -

potential in real space. However, due to the open boundary condition, the surface state wavefunctions vanish on the surface. If the impurity is located exactly on the surface, then it will not cause any scattering. This artifact can be cured by using a more realistic model to take into account the finite range of the impurity potential. Hence, we assume the following form of V_{imp} ,

$$V_{\text{imp}}(\vec{r}) = N_a V_0 e^{-z/a_0} \delta(x) \delta(y), \quad (26)$$

in which V_0 parameterizes the potential strength and N_a is a normalization factor. Although the detailed distribution of QPI patterns depends on the explicit form of V_{imp} , the overall characteristic features should not be sensitive on the choice of V_{imp} .

For an impurity whose spin is polarized in ν -direction with potential $V_{\text{imp}}(\vec{r})$, or, a non-magnetic impurity for $\nu = 0$, the retarded Green's function $\mathcal{G}_R^\nu(\omega, \vec{r})$ of the frequency ω at the position \vec{r} is defined by

$$\mathcal{G}_R^\nu(\omega, \vec{r}) = \langle \vec{r} | \frac{1}{\omega - (H + H_{\text{imp}}^\nu) + i\epsilon} | \vec{r} \rangle, \quad (27)$$

in which $|\vec{r}\rangle$ represents the coordinate eigen-state located at \vec{r} . In principle, \mathcal{G}_R^ν exhibits a matrix structure with respect to all the spin, Nambu, coordinate, and frequency indices. For $\mathcal{G}_R^\nu(\omega, \vec{r})$, it takes the diagonal elements in terms of coordinate and frequency, and leave the spin and Nambu indices general. H is the matrix-kernel of the B-deG Hamiltonian without impurity in Eq. (14) expressed in the coordinate representation. H_{imp}^ν is the impurity potential in the Nambu representation, defined as

$$H_{\text{imp}}^\nu = V_{\text{imp}}(\vec{r}) \Sigma^\nu, \quad (28)$$

where $\Sigma^\nu = \tau_3 \otimes S^\nu$ for $\nu = 0, 1, 3$, and $\Sigma^2 = \tau_0 \otimes S^2$. τ_3 is the Pauli matrix and τ_0 is the identity matrix acting in Nambu space, and S^0 is the identity matrix acting in spin space.

We define the 3D local density of states (LDOS) tensor as

$$\rho^{\mu\nu}(\omega, \vec{r}) = -\frac{1}{2\pi} \text{ImTr} \left((1 + \tau_3) \Sigma^\mu \mathcal{G}_R^\nu(\omega, \vec{r}) \right), \quad (29)$$

in which $1 + \tau_3$ is the abbreviation of $(I_2 + \tau_3) \otimes I_4$. $\rho^{\mu\nu}(\omega, \vec{r})$ refers to the density distribution in the presence of the magnetic or non-magnetic impurity for $\mu = 0$, and the spin-density distribution at polarization μ at $\mu \neq 0$. Then the surface LDOS tensor $\rho_{sf}^{\mu\nu}(\omega, \vec{r}_\parallel)$ for the position \vec{r}_\parallel on the surface is defined by

$$\rho_{sf}^{\mu\nu}(\omega, \vec{r}_\parallel) = \int d\vec{r} \mathcal{F}(\vec{r} - \vec{r}_c) \rho^{\mu\nu}(\omega, \vec{r}), \quad (30)$$

where $\vec{r}_c = (\vec{r}_\parallel, 0)$ is the 3D coordinate, and $\mathcal{F}(\vec{r} - \vec{r}_c)$ is an envelop function describing the sensitivity of the STM tip to the local density of state distribution along the z -axis. Here, we do not use the δ -function along the z -direction either, due to the open boundary condition used

for the calculation of surface states. Instead, a Gaussian distribution envelop function is used

$$\mathcal{F}(\vec{r}) = N_b e^{-(\frac{z}{\epsilon_0})^2} \delta(x) \delta(y), \quad (31)$$

in which N_b is the normalization factor. The characteristic features of the LODS should not be sensitive to the detailed form of the function \mathcal{F} .

Subtracting the background contribution in the absence of the impurity from $\rho_{sf}^{\mu\nu}(\omega, \vec{r}_\parallel)$, we extract the impurity contribution to the LDOS defined as

$$\Delta \rho_{sf}^{\mu\nu}(\omega, \vec{r}_\parallel) = -\frac{1}{2\pi i} \int_{-\infty}^0 dz \mathcal{F}(z) \text{Tr} \left[(1 + \tau_3) \Sigma^\mu \left(\Delta \mathcal{G}_R^\nu(\omega, \vec{r}_\parallel, z) - \Delta \mathcal{G}_R^{\nu*}(\omega, \vec{r}_\parallel, z) \right) \right], \quad (32)$$

where

$$\Delta \mathcal{G}_R^\nu(\omega, \vec{r}) = \mathcal{G}_R^\nu(\omega, \vec{r}) - \mathcal{G}_R^{(0)}(\omega, \vec{r}), \quad (33)$$

with

$$\mathcal{G}_R^{(0)}(\omega, \vec{r}) = \langle \vec{r} | \frac{1}{\omega - H + i\epsilon} | \vec{r} \rangle. \quad (34)$$

The QPI pattern in momentum space $\Delta \rho_{sf}^{\alpha\beta}(\omega, \vec{q})$ is defined to be the Fourier transform of $\Delta \rho_{sf}^{\alpha\beta}(\omega, \vec{r}_\parallel)$ with respect to \vec{r}_\parallel , as

$$\Delta \rho_{sf}^{\mu\nu}(\omega, \vec{q}) = -\frac{1}{2\pi i} \int_{-\infty}^0 dz \mathcal{F}(z) \left(\Lambda^{\mu\nu}(\omega, \vec{q}, z) - \Lambda^{\mu\nu*}(\omega, -\vec{q}, z) \right), \quad (35)$$

in which $\Lambda^{\mu\nu}(\omega, \vec{q}, z)$ is the Fourier transform of $\text{Tr}[(1 + \tau_3) \Sigma^\mu \Delta \mathcal{G}_R^\nu(\omega, \vec{r}_\parallel, z)]$.

B. The T -matrix formalism and Born approximation

The retarded Green's function $\mathcal{G}_R(\omega, \vec{r}_\parallel, z)$ can be evaluated using the T -matrix formalism. Define the operator $\mathcal{G}_R(\omega)$ as

$$\mathcal{G}_R(\omega) = \frac{1}{\omega - H - H_{\text{imp}} + i\epsilon}, \quad (36)$$

and that in the absence of impurity $\mathcal{G}_R^{(0)}(\omega)$ as

$$\mathcal{G}_R^{(0)}(\omega) = \frac{1}{\omega - H + i\epsilon}. \quad (37)$$

$\mathcal{G}_R(\omega)$ can be solved through

$$\mathcal{G}_R(\omega) = \mathcal{G}_R^{(0)}(\omega) + \mathcal{G}_R^{(0)}(\omega) T(\omega) \mathcal{G}_R^{(0)}(\omega), \quad (38)$$

in which the T -matrix operator $T(\omega)$ satisfies the equation

$$T(\omega) = H_{\text{imp}} + H_{\text{imp}} \mathcal{G}_R^{(0)}(\omega) T(\omega). \quad (39)$$

The Born approximation will be performed to solve the T -matrix.

Now we outline the procedure of calculating $\Delta\rho_{sf}^{\mu\nu}$ based on Eq. 35. First, $\Delta\mathcal{G}_R^\nu(\omega, \vec{q}, z)$ can be evaluated by inserting the complete basis to both the left and right hand sides of $T(\omega)$ in Eq. (38). A general eigenstate of the Hamiltonian H is of the form $\frac{1}{L}e^{i\vec{k}_\parallel \cdot \vec{r}_\parallel}\Psi_{\vec{k}_\parallel, \alpha}(z)$, where L stands for the average inter-impurity distance, and the index α labels the states with fixed in-surface momentum \vec{k}_\parallel , which can be either scattering state or surface state. $\Psi_{\vec{k}_\parallel, \alpha}(z)$ is the 8-component normalized wavefunction in z -direction. After carrying out the Fourier transform, we obtain

$$\begin{aligned} \Lambda^{\mu\nu}(\omega, \vec{q}, z) &= \frac{N_a}{L^2} \sum_{\vec{k}_\parallel, \alpha, \vec{k}'_\parallel, \beta} \delta_{\vec{k}_\parallel - \vec{k}'_\parallel, \vec{q}} \frac{1}{\omega - E_{\vec{k}_\parallel, \alpha} + i\epsilon} \\ &\times \langle \Psi_{\vec{k}_\parallel, \alpha} | H_{\text{imp}, z}^\nu | \Psi_{\vec{k}'_\parallel, \beta} \rangle \frac{1}{\omega - E_{\vec{k}'_\parallel, \beta} + i\epsilon} \\ &\times \text{Tr} \left[(1 + \tau_3) \Sigma^\mu \Psi_{\vec{k}_\parallel, \alpha}(z) \Psi_{\vec{k}'_\parallel, \beta}^\dagger(z) \right], \quad (40) \end{aligned}$$

in which $E_{\vec{k}_\parallel, \alpha}$ is the energy of the wavefunction $\Psi_{\vec{k}_\parallel, \alpha}(z)$, $H_{\text{imp}, z}^\nu(z)$ is the impurity potential in z -direction defined as $H_{\text{imp}, z}^\nu(z) = \Sigma^\nu V_0 e^{-z/a_0}$, and $\langle \Psi_{\vec{k}_\parallel, \alpha} | H_{\text{imp}, z}^\nu | \Psi_{\vec{k}'_\parallel, \beta} \rangle$ represents $\int_{-\infty}^0 dz V_0 e^{-z/a_0} \Psi_{\vec{k}_\parallel, \alpha}^\dagger(z) \Sigma^\nu \Psi_{\vec{k}'_\parallel, \beta}(z)$. In Eq. 40, the expression of $\Psi_{\vec{k}_\parallel, \alpha}(z) \Psi_{\vec{k}'_\parallel, \beta}^\dagger(z)$ represents a 8×8 matrix structure in the combined spin and Nambu space.

We consider the QPI patterns for at the frequency less than the gap energy. Since the density of states is singular at zero energy arising from the surface flat bands, only the Majorana zero modes are kept in the summation over states. With this approximation, Eq. (40) becomes

$$\begin{aligned} \Lambda^{\mu\nu}(\omega, \vec{q}, z) &= \frac{N_a}{N} \sum_{\vec{k}_\parallel, \vec{k}'_\parallel} \delta_{\vec{k}_\parallel - \vec{k}'_\parallel, \vec{q}} \left(\frac{1}{\omega + i\epsilon} \right)^2 \\ &\times \langle \Psi_{\vec{k}_\parallel}^M | H_{\text{imp}, z}^\nu | \Psi_{\vec{k}'_\parallel}^M \rangle \text{Tr} \left[(1 + \tau_3) \Sigma^\mu \Psi_{\vec{k}_\parallel}^M(z) \Psi_{\vec{k}'_\parallel}^{M\dagger}(z) \right], \quad (41) \end{aligned}$$

in which $\Psi_{\vec{k}_\parallel}^M(z)$ represents the wavefunction of the Majorana state with the in-plane momentum \vec{k}_\parallel .

The surface Majorana modes exhibit flat-band structure at zero energy. In the case of the dilute limit, in which the single impurity scattering can be justified, the scattering matrix element scales as V_0/L^2 , thus the scattering occurs nearly at zero energy. Below, we set ω at the order of ϵ , which can be viewed as the inverse lifetime of the Majorana states.

Before presenting the detailed QPI patterns, there is a general property of $\Delta\rho^{\mu\nu}(\omega, \vec{q})$. Since both the density and spin-density distributions are real fields, their Fourier transforms satisfy

$$\Delta\rho^{\mu\nu}(\omega, \vec{q}) = \Delta\rho^{\mu\nu*}(\omega, -\vec{q}). \quad (42)$$

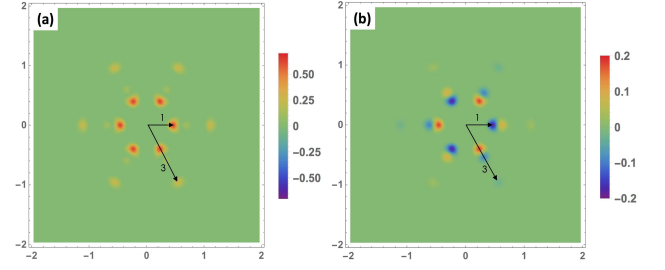


FIG. 6: $a)$ $\text{Re}\Delta\rho_{sf}^{00}(\epsilon, \vec{q})$ and $b)$ $\text{Im}\Delta\rho_{sf}^{00}(\epsilon, \vec{q})$ in the (111)-surface for $\Delta_s/\Delta_p = 0.3$ under the Born approximation. The background contribution in the absence of impurity is subtracted. The numerical computations are carried out for a 60×60 lattice in momentum space. The tip resolution b_0 in Eq. (31) is set to be $b_0 = 1/(\sqrt{2}k_f)$, and the impurity range a_0 in Eq. (26) is taken as $a_0 = 1/(\sqrt{2}k_f)$, both of which are at the order of Fermi wavelength. The impurity potential strength is taken as $V_0 = g\Delta_0$ where g is a scaling factor satisfying $g \ll 1$ to justify the Born approximation. Other parameters are $\lambda_1 = 0, \lambda_2 = |\mu|/(2k_f^2)$, and $\lambda_3 = 0$. $\Delta_0 = 0.02|\mu|$, $N_a = \frac{1}{2k_f^2}$, $N_b = \sqrt{2}k_f$. $\epsilon = 2 \times 10^{-5}|\mu|$, which is the inverse of the Majorana life time. The color bar is in the unit of $g \frac{\sqrt{2}k_f}{800\pi^2|\mu|}$.

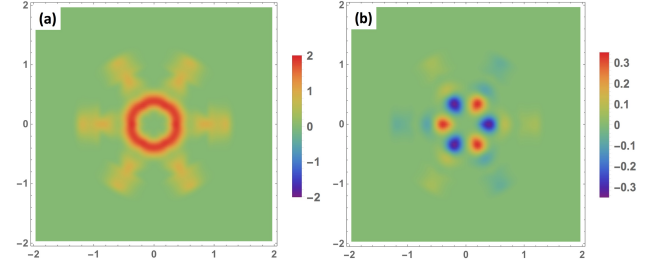


FIG. 7: $a)$ $\text{Re}\Delta\rho_{sf}^{00}(\epsilon, \vec{q})$ and $b)$ $\text{Im}\Delta\rho_{sf}^{00}(\epsilon, \vec{q})$ in the (111)-surface with the parameter $\Delta_s/\Delta_p = 0.7$. The other parameters are as the same as in Fig. 6.

In other words, $\text{Re}\Delta\rho^{\mu\nu}(\omega, \vec{q})$ and $\text{Im}\Delta\rho^{\mu\nu}(\omega, \vec{q})$ are even and odd with respect to \vec{q} . This symmetry has been clearly shown in all of Fig. 6, Fig. 7, Fig. 8, and Fig. 9, which present the Fourier transforms of $\Delta\rho_{sf}^{\mu\nu}(\omega, \vec{q})$ at $\omega = \epsilon$ in (111)-surface.

C. The QPI pattern for a non-magnetic impurity

In this section, the QPI patterns for non-magnetic impurities are presented. $\Delta\rho_{sf}^{\mu 0}(\omega, \vec{q})$ vanishes when $\mu \neq 0$ due to TR symmetry, hence, only the results of $\Delta\rho_{sf}^{00}(\omega, \vec{q})$ are displayed.

Fig. 6 and Fig. 7 present $\Delta\rho_{sf}^{00}(\omega, \vec{q})$ at two representative pairing ratios Δ_s/Δ_p . Both figures exhibit the C_{3v} symmetry with three vertical reflection planes. For a non-magnetic impurity, the Hamiltonian remains odd under the chiral operation defined in Eq. (25), which imposes strong restrictions on the QPI patterns. It can only

couple the Majorana zero modes with opposite chiral indices as shown in Fig. 4 (a) and (b). In Fig. 4 (a), four representative scattering wavevectors between Majorana islands are drawn in red arrowed lines, among which “0” represents the intra-island scattering, and “1”, “2”, and “3” represent inter-island scatterings. The scatterings “1” and “3” are between islands with opposite chiral indices, hence are allowed in the Born approximation, as shown in Fig. 6. In contrast, the scatterings of “0” and “2” connect islands with the same chiral index, and hence are forbidden. For example, the QPI spectra vanish near $q = 0$, which is the consequence of the absence of intra-island scatterings.

While both scatterings “1” and “3” appear in the QPI patterns, the QPI spectral magnitudes of “3” are much weaker than that of “1”, which is a consequence of TR symmetry. The impurity matrix element vanishes between two Majorana states with in-plane momenta \vec{k}_{2d} and \vec{k}'_{2d} with $\vec{k}'_{2d} = -\vec{k}_{2d}$, forming a Kramers pair with $T^2 = -1$. Nevertheless, the TR symmetry does not completely forbid the scattering from \vec{k}_{2d} to \vec{k}'_{2d} in the neighbourhood of $-\vec{k}_{2d}$, although this kind of scatterings are weakened. Hence, unlike the case of chiral symmetry which completely forbids scatterings between islands with the same chiral index, the TR symmetry only reduces while not strictly forbids the scatterings between TR related Majorana islands. For the case of a large pairing ratio Δ_s/Δ_p as shown in Fig. 7, the phase space for non-TR related Majorana states scatterings for inter-island scattering “3” is much larger than the case shown in Fig. 6.

D. The QPI for a magnetic impurity

In this part, the QPI patterns for the magnetic impurity are presented, corresponding to $\Delta\rho_{sf}^{\mu\nu}(\omega, \vec{q})$ with $\nu \neq 0$. The magnetic impurity may also trap the Yu-Shiba bound states. The number of such states are finite, and their spatial distributions are only localized around the magnetic impurities. They exhibit sharp resonance peaks in the LDOS in the STM spectra around the impurity. However, the QPI spectra are the Fourier transform of LDOS over a large area, which are mostly related to the scattering states. Hence, the Yu-Shiba states can be neglected in calculating the QPI spectra without affecting any characteristic features. Nevertheless, their possible existence is certainly an interesting question worthwhile for a future investigation.

The magnetic impurity is assumed to be in the classical limit without fluctuations. Although in principle, a magnetic impurity could also induce the density response, it is a high order effect not showing up at the level of the second order Born approximation. Only $\mu, \nu \neq 0$ are displayed here. For simplicity, we will use Latin indices to refer spin directions 1, 2, 3.

Fig. 8 and 9 show the real and imaginary parts of

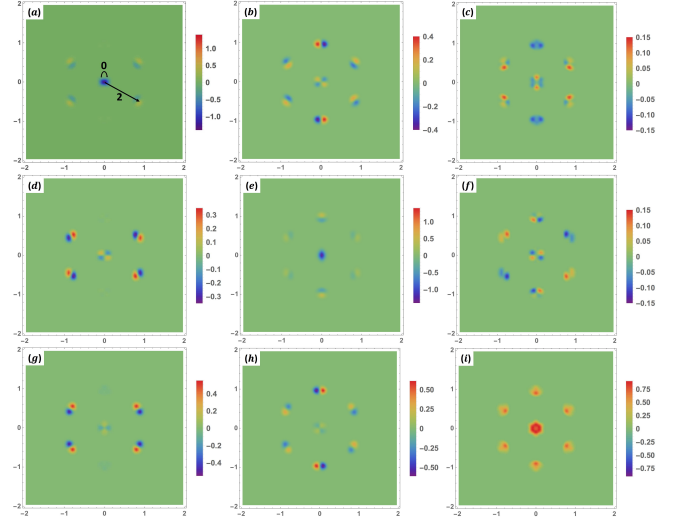


FIG. 8: $\text{Re}\Delta\rho_{sf}^{ij}(\epsilon, \vec{q})$ with ij equal to a)11, b)12, c)13, d)21, e)22, f)23, g)31, h)32, i)33, for $\Delta_s/\Delta_p = 0.3$ in the (111)-surface. The background contribution in the absence of impurity is subtracted. The numerical computations are carried out for a 60×60 lattice in momentum space. The parameters are taken the same as Fig. 6.

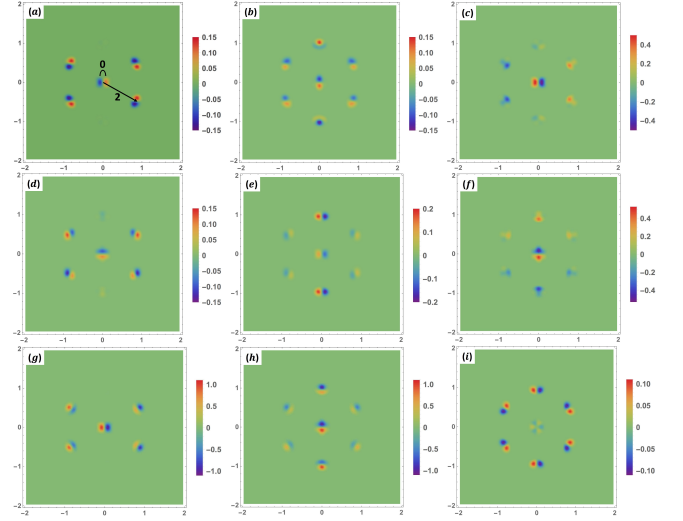


FIG. 9: $\text{Im}\Delta\rho_{sf}^{ij}(\epsilon, \vec{q})$ with ij equal to a) 11, b) 12, c) 13, d) 21, e) 22, f) 23, g) 31, h) 32, i) 33. The parameters are the same as those in Fig. 6.

$\Delta\rho_{sf}^{ij}(\epsilon, \vec{q})$, respectively. The magnetic impurity Hamiltonian H_{imp}^j ($j = 1, 2, 3$) is even under the chiral operation, hence, it only induces scatterings between Majorana islands with the same chiral index denoted as scatterings “0” and “2” in Fig. 4. For example, these two classes of scatterings are marked in the QPI patterns of $\Delta\rho_{sf}^{11}(\omega, \vec{q})$ shown in Fig. 8 (a) and Fig.9 (a).

The consequences of the point group symmetry are more complicated. Let us first consider the magnetic impurity with spin oriented along the z -direction, the

impurity Hamiltonian still preserves the C_3 symmetry. Hence, the QPI patterns of $\Delta\rho^{33}(\epsilon, \vec{q})$ explicitly exhibit the C_3 symmetry as shown in Fig. 8 (i) and Fig. 9 (i). As for $\Delta\rho^{13}(\epsilon, \vec{q})$ and $\Delta\rho^{23}(\epsilon, \vec{q})$, their symmetry properties under the C_3 rotation

$$\Delta\rho^{i3}(\epsilon, R\vec{q}) = R_{ij}\Delta\rho^{j3}(\epsilon, \vec{q}), \quad (43)$$

where R_{ij} refers to the 2×2 rotation matrix of a C_3 rotation. For example, for the rotation $R(\hat{z}, \frac{2\pi}{3})$, $\Delta\rho^{i3}$ satisfies

$$\begin{pmatrix} \Delta\rho^{13}(\epsilon, \vec{q}) \\ \Delta\rho^{23}(\epsilon, \vec{q}) \end{pmatrix} = \frac{1}{2} \begin{pmatrix} -1 & \sqrt{3} \\ -\sqrt{3} & -1 \end{pmatrix} \begin{pmatrix} \Delta\rho^{13}(\epsilon, \vec{q}') \\ \Delta\rho^{23}(\epsilon, \vec{q}') \end{pmatrix}, \quad (44)$$

where $\vec{q}' = R(\hat{z}, \frac{2\pi}{3})\vec{q}$, and this property has been checked for Fig. 8 (c, f) and Fig. 9 (c, f). On the other hand, the vertical reflection symmetry with respect to xz -plane is broken, nevertheless, it can be restored by combining with TR operation. S^z and S^x are odd for this operation, while S^y is even, hence,

$$\Delta\rho^{i3}(\epsilon, \vec{q}) = \pm\Delta\rho^{i3}(\epsilon, \vec{q}'), \quad (45)$$

where $+$ applies for $i = x, z$ and $-$ applies for $i = y$; \vec{q}' is the image of \vec{q} after the reflection. Similar transformations can be derived for other planes equivalent to the xz -plane by the C_3 rotations. It is easy to check that all of Fig. 8 (c, f, i) and 9 (c, f, i) satisfy these properties.

Now we consider the case of the impurity spin orientation along the x -direction. Then the C_3 rotation symmetry is no long kept. The symmetry of the combined reflection followed by TR operation is still valid, nevertheless, the reflection plane can only be the xz -plane. Hence, we have

$$\Delta\rho^{i1}(\epsilon, \vec{q}) = \pm\Delta\rho^{i1}(\epsilon, \vec{q}'), \quad (46)$$

where $+$ applies for $i = x, z$, and $-$ applies for $i = y$. Again this can be checked by examining Fig. 8 (a, d, g) and Fig. 9 (a, d, g). At last, we examine the case of the impurity spin orientation along the y -direction. Again the C_3 rotation symmetry is lost, while the reflection symmetry with respect to the xz -plane is maintained.

$$\Delta\rho^{i2}(\epsilon, \vec{q}) = \mp\Delta\rho^{i2}(\epsilon, \vec{q}'), \quad (47)$$

where $-$ applies for $i = x, z$, and $+$ applies for $i = y$. Clearly this symmetry is respected in Fig. 8 (b, e, h) and Fig. 9 (b, e, h).

VI. SUMMARY

In summary, the non-centrosymmetric effective spin- $\frac{3}{2}$ systems with cubic group symmetries are discussed. The emphasis is put on the T_d group, which is relevant to the YPtBi material. The double degeneracy along $[001]$ and equivalent directions for systems with T_d symmetry is shown to be protected by the little group SD_{16} .

Majorana surface states are calculated for the proposed mixed s -wave singlet and p -wave septet pairing of the T_d case in (111)-surface. Two representative values of the ratio between s - and p -wave pairing components are taken as examples for calculations. The Majorana states form flat bands within the regions enclosed by the projections of the nodal loops in gap functions on the surface Brillouin zone, but disappear in the overlapping regions. The results are consistent with the bulk-edge correspondence principle. The QPI patterns are computed for the surface states with a single impurity in Born approximation. Chiral symmetry forbids scatterings between Majorana islands of same (opposite) chiral index for the non-magnetic (magnetic) impurities. There are richer structures in the QPI patterns under the transformation of C_{3v} group for the case of magnetic impurity than the case of non-magnetic impurity. Experimental signatures on the QPI patterns can test the possible mixed s, p pairing for the half-Heusler compound YPtBi.

Acknowledgments. W. Y. and C. W. acknowledge the support from the NSF DMR-1410375 and AFOSR FA9550-14-1-0168. T. X is supported by National Key R&D Program of China 2017YFA0302901 and National Natural Science Foundation of China Grant No 11474331. C. W. also acknowledges the support from the National Natural Science Foundation of China (11729402).

Note added. Near the completion of this manuscript, we learned the recent works on superconductivity on the half-Heusler material⁵⁸⁻⁶⁰.

Appendix A: Invariants of the cubic groups

In this appendix, we briefly describe the five cubic point groups O_h , O , T_d , T_h , T , then classify the spherical harmonics of momentum and spin tensors up to the third rank according to their irreducible representations. All cubic-group-symmetry invariants up to the third rank of momentum and spin tensors are presented.

Let us recall some group theory knowledge. The O_h group is the symmetry group of the cube, containing 48 elements, hence, is the largest one among the five cubic groups. The other four are its subgroups, which are the symmetry groups of decorated cubes in different ways. Fig. 2 shows the case of the T_d group. In the designated coordinate system, O is at the origin. Among the eight vertices, A, B, C, D are located at $(-1, -1, -1)$, $(1, -1, 1)$, $(1, 1, -1)$ and $(-1, 1, 1)$, respectively, and A', B', C', D' are their inversion symmetric partners, respectively. We use \mathcal{I} to denote the inversion operation, and $R(\hat{n}, \theta)$ the rotation around the direction \hat{n} by the angle θ . The group O_h has 24 proper elements, which corresponds to rotations, and their conjugation classes E , $3C_2$, $6C_4$, $6C_2'$ and $8C_3$ are listed in Table I. The other 24 elements are improper operations corresponding to combinations of rotation and inversion. Their conjugation classes are i , $3\sigma_h$, $6S_4$, $6\sigma_d$, and $8S_6$ by applying the inversion operation to E , $3C_2$, $6C_4$, $6C_2'$ and

E	1	(x, y, z)	identity
$3C_2$	2	$(x, -y, -z)$	$R(OX, \pi)$
	3	$(-x, y, -z)$	$R(OY, \pi)$
	4	$(-x, -y, z)$	$R(OZ, \pi)$
$6C_4$	5	$(x, z, -y)$	$R(OX', \frac{\pi}{2})$
	6	$(x, -z, y)$	$R(OX'', \frac{\pi}{2})$
	7	$(-z, y, x)$	$R(OY', \frac{\pi}{2})$
	8	$(z, y, -x)$	$R(OY'', \frac{\pi}{2})$
	9	$(y, -x, z)$	$R(OZ', \frac{\pi}{2})$
	10	$(-y, x, z)$	$R(OZ'', \frac{\pi}{2})$
$6C_2'$	11	$(y, x, -z)$	$R([AC], \pi)$
	12	$(-y, -x, -z)$	$R([BD], \pi)$
	13	$(z, -y, x)$	$R([AB], \pi)$
	14	$(-z, y, -x)$	$R([CD], \pi)$
	15	$(-x, z, y)$	$R([AD], \pi)$
	16	$(-x, -z, -y)$	$R([BC], \pi)$
$8C_3$	17	(y, z, x)	$R(OA, \frac{2\pi}{3})$
	18	(z, x, y)	$R(OA', \frac{2\pi}{3})$
	19	$(-y, -z, x)$	$R(OB, \frac{2\pi}{3})$
	20	$(z, -x, -y)$	$R(OB', \frac{2\pi}{3})$
	21	$(y, -z, -x)$	$R(OC, \frac{2\pi}{3})$
	22	$(-z, x, -y)$	$R(OC', \frac{2\pi}{3})$
	23	$(-y, z, -x)$	$R(OD, \frac{2\pi}{3})$
	24	$(-z, -x, y)$	$R(OD', \frac{2\pi}{3})$

TABLE I: List of 24 group elements of point group O . In accordance with the notations in Fig. 2, OM represents the vector pointing from the center of the cube (i.e. the point O) to the vertex or the direction M , where M is one of $A, A', B, B', C, C', D, D'$ when it is a vertex of the cube, and is one of X, Y, Z, X', Y', Z' when it represents a direction. X, Y, Z represent the positive directions of the three axes x, y, z , and X', Y', Z' represent the negative directions of the three axes. The symbol $[MN]$ represents the line passing through the point that bisects the edge MN' and the point that bisects $M'N$, where M, N, M', N' are all vertices of the cube.

	O_h	O	T_d	T_h	T
$\{k_i\}_{1 \leq i \leq 3}$	T_{1u}	T_1	T_2	T_u	T
$k_x^2 + k_y^2 + k_z^2$	A_{1g}	A_1	A_1	A_g	A
$\{(k_x^2 + k_y^2 - 2k_z^2)/\sqrt{2}, k_x^2 - k_y^2\}$	E_g	E	E	E_g	E
$\{k_i k_{i+1}\}_{1 \leq i \leq 3}$	T_{2g}	T_2	T_2	T_g	T
$k_x k_y k_z$	A_{2u}	A_2	A_1	A_u	A
$\{k_i^3\}_{1 \leq i \leq 3}$	T_{1u}	T_1	T_2	T_u	T
$\{k_i(k_{i+1}^2 + k_{i+2}^2)\}_{1 \leq i \leq 3}$	T_{1u}	T_1	T_2	T_u	T
$\{k_i(k_{i+1}^2 - k_{i+2}^2)\}_{1 \leq i \leq 3}$	T_{2u}	T_2	T_1	T_u	T

TABLE II: Classifications of the momentum spherical harmonics up to the cubic order according to irreducible representations of the five cubic point groups. The subscripts $i, i+1, i+2$ are defined cyclically in x, y, z .

$8C_3$, respectively. For simplicity, they are not listed. The other four cubic groups are subgroups of O_h represented

	O_h	O	T_d	T_h	T
$\{S_i\}_{1 \leq i \leq 3}$	T_{1g}	T_1	T_1	T_g	T
$\{(S_x^2 + S_y^2 - 2S_z^2)/\sqrt{2}, S_x^2 - S_y^2\}$	E_g	E	E	E_g	E
$\{S_i S_{i+1} + S_{i+1} S_i\}_{1 \leq i \leq 3}$	T_{2g}	T_2	T_2	T_g	T
$\text{Sym}(S_x S_y S_z)$	A_{2g}	A_2	A_2	A_g	A
$\{S_i^3\}_{1 \leq i \leq 3}$	T_{1g}	T_1	T_1	T_g	T
$\{S_{i+1} S_i S_{i+1} - S_{i+2} S_i S_{i+2}\}_{1 \leq i \leq 3}$	T_{2g}	T_2	T_2	T_g	T

TABLE III: Classifications of spin tensors up to the third rank according to the irreducible representations of the five cubic groups. The symbol "Sym" represents symmetrization as a sum of all permutations of the objects inside the symbol. The subscripts $i, i+1, i+2$ are defined cyclically in x, y, z .

	O_h	O	T_d	T_h	T
$k_x k_y k_z \cdot \text{Sym}(S_x S_y S_z)$	A_{1u}	A_1	A_2	A_u	A
$k_i \cdot S_i$	A_{1u}	A_1	A_2	A_u	A
$k_i \cdot S_i^3$	A_{1u}	A_1	A_2	A_u	A
$k_i \cdot (S_{i+1} S_i S_{i+1} - S_{i+2} S_i S_{i+2})$	A_{2g}	A_2	A_1	A_u	A
$k_i^3 \cdot S_i$	A_{1u}	A_1	A_2	A_u	A
$k_i^3 \cdot S_i^3$	A_{1u}	A_1	A_2	A_u	A
$k_i^3 \cdot (S_{i+1} S_i S_{i+1} - S_{i+2} S_i S_{i+2})$	A_{2g}	A_2	A_1	A_u	A
$k_i(k_{i+1}^2 + k_{i+2}^2) \cdot S_i$	A_{1u}	A_1	A_2	A_u	A
$k_i(k_{i+1}^2 + k_{i+2}^2) \cdot S_i^3$	A_{1u}	A_1	A_2	A_u	A
$k_i(k_{i+1}^2 + k_{i+2}^2) \cdot (S_{i+1} S_i S_{i+1} - S_{i+2} S_i S_{i+2})$	A_{2g}	A_2	A_1	A_u	A
$k_i(k_{i+1}^2 - k_{i+2}^2) \cdot S_i$	A_{2u}	A_2	A_1	A_u	A
$k_i(k_{i+1}^2 - k_{i+2}^2) \cdot S_i^3$	A_{2u}	A_2	A_1	A_u	A
$k_i(k_{i+1}^2 - k_{i+2}^2) \cdot (S_{i+1} S_i S_{i+1} - S_{i+2} S_i S_{i+2})$	A_{1u}	A_1	A_2	A_u	A

TABLE IV: The TR and rotation-invariant combinations of momentum and spin tensors up to the third rank. The second rank combinations preserving the inversion symmetry are not shown since they have been already included in the Luttinger-Kohn Hamiltonian. "." represents the inner product as a summation of i from 1 to 3.

by the conjugation classes as

$$\begin{aligned}
O &= \{E, 3C_2, 6C_4, 6C_2', 8C_3\}, \\
T_d &= \{E, 3C_2, 8C_3, 6S_4, 6\sigma_d\}, \\
T_h &= \{E, 3C_2, 8C_3, i, 3\sigma_h, 8S_6\}, \\
T &= \{E, 3C_2, 8C_3\}.
\end{aligned} \tag{A1}$$

In Table II, we list all the momentum harmonics up to the third rank. There are three, six, and ten harmonics for rank-1, 2 and 3, respectively. The decompositions to cubic groups are rank-1 = T , rank-2 = $A \oplus E \oplus T$, and rank-3 = $A \oplus T \oplus T \oplus T$. For different groups, A and T can be further classified to $A_{1,2}$, and $T_{1,2}$, respectively. For groups containing inversion operation, the sub-index g and u mean representations of even and odd parities, respectively. The spherical spin tensors are presented in Tab. III. Since $\sum_i S_i^2 = S(S+1)$, there are only 5 and 7 independent spin tensors at rank-2 and 3, respectively. Since spin operators are parity even, all the corresponding representations are of the g -type.

Here we list all spin-orbit coupled invariants up to the third order in momentum for three inversion-breaking cu-

bic groups O, T_d, T . For the point group O , the invariants are

$$\begin{aligned} & k_i \cdot S_i, \quad k_i \cdot S_i^3, \\ & k_x k_y k_z \text{Sym}(S_x S_y S_z), \\ & k_i^3 \cdot S_i, \quad k_i^3 \cdot S_i^3, \\ & k_i(k_{i+1}^2 + k_{i+2}^2) \cdot S_i, \quad k_i(k_{i+1}^2 + k_{i+2}^2) \cdot S_i^3, \\ & k_i(k_{i+1}^2 - k_{i+2}^2) \cdot (S_{i+1} S_i S_{i+1} - S_{i+2} S_i S_{i+2}). \end{aligned} \quad (\text{A2})$$

The T_d invariants are

$$\begin{aligned} & k_i \cdot (S_{i+1} S_i S_{i+1} - S_{i+2} S_i S_{i+2}), \\ & k_i^3 \cdot (S_{i+1} S_i S_{i+1} - S_{i+2} S_i S_{i+2}), \\ & k_i(k_{i+1}^2 - k_{i+2}^2) \cdot S_i, \quad k_i(k_{i+1}^2 - k_{i+2}^2) \cdot S_i^3, \\ & k_i(k_{i+1}^2 + k_{i+2}^2) \cdot (S_{i+1} S_i S_{i+1} - S_{i+2} S_i S_{i+2}). \end{aligned} \quad (\text{A3})$$

For T , all the invariants of O and T_d are allowed. In these expressions, the dot “ \cdot ” represents an inner product between the two 3-vectors, in which “ i ” runs over x, y, z and a summation $\sum_{i=x,y,z}$ is taken. Inversion symmetry is explicitly broken by all the terms, hence the double degeneracy in the heavy hole and light hole bands is in general absent.

The TR symmetry requires that the homogeneity of the combinations be even. The inversion-preserving combinations have already been included in the Luttinger-Kohn Hamiltonian Eq. (5). There are 17 inversion breaking combinations which are listed in Table IV. All of these combinations belong to A -representations of the cubic groups. Whether they are A_1 , A_2 , or A_g , A_u of a particular cubic group can be obtained from the information in Tab. II and III and the multiplication rules of the representations.

Appendix B: The semi-dihedral group SD_{16}

In this appendix, we discuss the little group structure along the $[001]$ and its equivalent directions of the lattice system with the T_d symmetry augmented by spinor representations and TR symmetry. This little group is isomorphic to the semi-dihedral group (also called the quasi-dihedral group) SD_{16} , where the subscript “16” represents the order of the group.

With the T_d group, its little group L_0 along the $[001]$ direction is

$$L_0 = \{\mathbb{1}, M_{x'}, M_{y'}, R(\vec{z}, \pi)\}, \quad (\text{B1})$$

in which $\mathbb{1}$ is the identity element, and the directions of x' and y' are given in Fig. 2. The reflection $M_{x'}$ can be decomposed as $M_{x'} = \mathcal{I}R(\hat{x}', \pi)$. L_0 is isomorphic to D_2 , the dihedral group of order 4, which is Abelian and only has 1D irreducible representations.

For half-spin fermions, L_0 needs to be doubled to L_1 by adding $\bar{\mathbb{1}} = R(\vec{n}, 2\pi)$, then L_1 is represented by

$$\begin{aligned} L_1 = \{ & \mathbb{1}, M_{x'}, M_{y'}, R(\vec{z}, \pi), \\ & \bar{\mathbb{1}}, \bar{\mathbb{1}}M_{x'}, \bar{\mathbb{1}}M_{y'}, \bar{\mathbb{1}}R(\vec{z}, \pi)\}. \end{aligned} \quad (\text{B2})$$

$\bar{\mathbb{1}}$ commutes with every element in the group, which takes -1 for half-integer spin representations. Since the inversion operator \mathcal{I} commutes with all $O(3)$ elements and acts as identity operator in spin space, we can explicitly check that

$$\begin{aligned} M_{x'}^2 &= R(\hat{x}', 2\pi) = \bar{\mathbb{1}}, \\ M_{x'} M_{y'} &= R(\vec{z}, \pi) = -M_{y'} M_{x'}, \end{aligned} \quad (\text{B3})$$

hence L_1 is non-Abelian. We can explicitly work out the multiplication rules of L_1 , which shows that it is isomorphic to the quaternion group,

$$Q_8 = \{\pm 1, \pm i, \pm j, \pm k\}, \quad (\text{B4})$$

through the identifications $\mathbb{1} = 1$, $\bar{\mathbb{1}} = -1$, $M_{x'} = i$, $M_{y'} = j$, and $R(\vec{z}, \pi) = k$. The multiplication rules of Q_8 are given by

$$\begin{aligned} i^2 &= j^2 = k^2 = -1, \\ ij &= -ji = k, jk = -kj = i, ki = -ik = j. \end{aligned} \quad (\text{B5})$$

Q_8 and hence L_1 has one 2D irreducible representations up to isomorphism in which $\mathbb{1}$ and $\bar{\mathbb{1}}$ take the value of 1 and -1 , respectively. and four 1D irreducible representations in which $\mathbb{1}$ and $\bar{\mathbb{1}}$ are identical.

Now we extend T_d to its magnetic group, and identify its little group along the $[001]$ -direction. The anti-unitary operator \mathcal{S} defined in Eq. 11 as $\mathcal{S} = R(\hat{z}, \frac{\pi}{2})\mathcal{T}'$ is an element of this little group, where $\mathcal{T}' = \mathcal{I}\mathcal{T}$. \mathcal{T}' leaves the momentum direction $[001]$ -direction unchanged, and $\mathcal{T}'^2 = 1$ or -1 depending on whether the spin is integer or half-odd integer. In the case of $\mathcal{T}'^2 = 1$, the magnetic little group is denoted as L_2

$$\begin{aligned} L_2 = \{ & \mathbb{1}, M_{x'}, M_{y'}, R(\vec{z}, \pi), \\ & \mathcal{S}, M_{x'}\mathcal{S}, M_{y'}\mathcal{S}, R(\vec{z}, \pi)\mathcal{S}\}. \end{aligned} \quad (\text{B6})$$

Defining $r = R(\hat{z}, \frac{\pi}{2})\mathcal{T}'$, $s = M_{x'}$, L_2 can be rewritten as

$$L_2 = \{1, r, r^2, r^3, s, sr, sr^2, sr^3\}, \quad (\text{B7})$$

which is isomorphic to D_4 , the dihedral group of order 4, with the relations of $r^4 = s^2 = 1$, $sr s^{-1} = r^{-1}$.

Finally we consider the case of $\mathcal{T}'^2 = -1$. We define r' as the spinor version of r and $s' = r' M_{x'}$. Then the magnetic little group L_3 for the $[001]$ -direction can be represented in terms of r' and s' as

$$\begin{aligned} L_3 = \{ & \mathbb{1}, r', r'^2, r'^3, \\ & r'^4, r'^5, r'^6, r'^7, \\ & s', s'r', s'r'^2, s'r'^3, \\ & s'r'^4, s'r'^5, s'r'^6, s'r'^7\}. \end{aligned} \quad (\text{B8})$$

This is in fact isomorphic to the semi-dihedral group SD_{16} of order 16 defined in terms of generators and relations as

$$SD_{16} = \langle r', s' | r'^8 = s'^2 = 1, s'r's'^{-1} = r'^3 \rangle. \quad (\text{B9})$$

Here we show that $s'r's'^{-1} = r^3$ as follows,

$$\begin{aligned}
s'r's'^{-1} &= M_{x'}r'M_{x'}^{-1}\mathcal{T}' \\
&= R(\hat{x}', \pi)R(\hat{z}, \frac{\pi}{2})R(\hat{x}', \pi)^{-1}\mathcal{T}' \\
&= R(\hat{z}, \frac{7}{2}\pi)\mathcal{T}' = \bar{\mathbb{I}}R(\hat{z}, \frac{\pi}{2}\pi)\mathcal{T}' \\
&= R(\hat{z}, \frac{3}{2}\pi)\mathcal{T}'^3 = r'^3, \tag{B10}
\end{aligned}$$

in which in the second last line $R(\hat{z}, 2\pi) = \bar{\mathbb{I}}$ is used. We further note that SD_{16} has both Q_8 and D_4 as subgroups. The Q_8 subgroup is generated by $\{r'^2, r's'\}$, while the D_4 subgroup is generated by $\{r'^2, s'\}$.

Appendix C: The anti-unitary operator \mathcal{S} with $\mathcal{S}^4 = -1$

In this appendix, we will give the explicit form of the operator \mathcal{S} , and its action on the two doubly degenerate subspaces along $[001]$ directions.

Since \mathcal{I} acts as identity operator in the spin space, the anti-unitary operation \mathcal{S} is given by

$$\mathcal{S} = e^{-iS_z(-\pi/2)}R \cdot K, \tag{C1}$$

in which K is the complex conjugate operation. Then \mathcal{S} is computed as $\mathcal{S} = MK$, where

$$M = \begin{pmatrix} 0 & 0 & 0 & e^{i\frac{3\pi}{4}} \\ 0 & 0 & -e^{i\frac{\pi}{4}} & 0 \\ 0 & e^{-i\frac{\pi}{4}} & 0 & 0 \\ -e^{-i\frac{3\pi}{4}} & 0 & 0 & 0 \end{pmatrix}. \tag{C2}$$

It is straightforward to verify that $\mathcal{S}^2 = \text{diag}\{i, -i, i, -i\}$, and $\mathcal{S}^4 = -1$.

Up to an overall factor, the Hamiltonian Eq. (6) along the $[001]$ -direction is

$$H_z = S_z^2 + \delta(S_x S_z S_x - S_y S_z S_y), \tag{C3}$$

in which $|\delta| \ll 1$ for the case of small inversion breaking strength. Since the Hamiltonian Eq. (C3) changes the S_z -eigenvalue by 0 or 2, the helicity $\frac{3}{2}$ component will mix with the helicity $-\frac{1}{2}$ component, and similarly, the helicity $\frac{1}{2}$ -component mixes with the helicity $-\frac{3}{2}$ component.

As proved in Sect. II C, the spectra of Eq. C3 are doubly degenerate. The two eigenvectors $v_{1,2}$ corresponding to $E_v = \frac{1}{4}(5 + 2\sqrt{4 + 3\delta^2})$ are

$$\begin{aligned}
v_1 &= \frac{1}{\mathcal{N}} \left(1, 0, \frac{2}{\sqrt{3}\delta} \left(\sqrt{1 + \frac{3}{4}\delta^2} - 1 \right), 0 \right)^T, \\
v_2 &= \frac{1}{\mathcal{N}} \left(0, -\frac{2}{\sqrt{3}\delta} \left(\sqrt{1 + \frac{3}{4}\delta^2} - 1 \right), 0, 1 \right)^T, \tag{C4}
\end{aligned}$$

in which \mathcal{N} is the normalization factor. The two eigenvectors $w_{1,2}$ of $E_w = \frac{1}{4}(5 - 2\sqrt{4 + 3\delta^2})$ are

$$\begin{aligned}
w_1 &= \frac{1}{\mathcal{N}} \left(0, 1, 0, \frac{2}{\sqrt{3}\delta} \left(\sqrt{1 + \frac{3}{4}\delta^2} - 1 \right) \right)^T, \\
w_2 &= \frac{1}{\mathcal{N}} \left(-\frac{2}{\sqrt{3}\delta} \left(\sqrt{1 + \frac{3}{4}\delta^2} - 1 \right), 0, 1, 0 \right)^T. \tag{C5}
\end{aligned}$$

The anti-unitary operation \mathcal{S} is diagonal-blocked. Its off-diagonal elements between the two subspaces spanned by $v_{1,2}$ and $w_{1,2}$ are zero. In the subspace spanned by $v_{1,2}$ and that by $w_{1,2}$, it has matrix structure as

$$\mathcal{S} = \begin{pmatrix} 0 & e^{i\pm\frac{\pi}{4}} \\ -e^{-i\mp\frac{\pi}{4}} & 0 \end{pmatrix} K, \tag{C6}$$

in which the upper sign is for subspace $v_{1,2}$ and lower sign for $w_{1,2}$.

Appendix D: Topological index for nodal-line superconductors

In this appendix, we first review the definition of the path-dependent topological number for the TR invariant nodal topological superconductors²⁴, then apply it to the spin-3/2 case of the current interest. The pairing strengths of s - and p -wave components are parametrized as $\Delta_s = C_s \Delta_0$ and $\Delta_p = C_p \Delta_0$.

In the presence of TR symmetry, the combined operation $C = P_h T$, dubbed as chiral operator, anti-commutes with the B-deG Hamiltonian. As a result, $H_{\vec{k}}$ can be transformed into a block-off-diagonal form as

$$W H_{\vec{k}} W^\dagger = \begin{pmatrix} 0 & D_{\vec{k}}^\dagger \\ D_{\vec{k}} & 0 \end{pmatrix}. \tag{D1}$$

The matrix $D_{\vec{k}}$ can be decomposed into $D_{\vec{k}} = U_{\vec{k}} \Lambda_{\vec{k}} V_{\vec{k}}$ via singular-value decomposition, in which $\Lambda_{\vec{k}}$ is a diagonal matrix with non-negative eigenvalues, and $U_{\vec{k}}, V_{\vec{k}}$ are unitary matrices. Consider a closed path \mathcal{L} in momentum space. If the gap does not vanish along the path \mathcal{L} , then $\Lambda_{\vec{k}}$ on \mathcal{L} can be deformed into the identity matrix, and then $D_{\vec{k}}$ becomes a unitary matrix denoted as $Q_{\vec{k}}$. The topological number of the path \mathcal{L} is defined by the formula²⁴,

$$N_{\mathcal{L}} = \frac{1}{2\pi i} \int_{\mathcal{L}} dk_l \text{Tr}[Q_{\vec{k}}^\dagger \partial_{k_l} Q_{\vec{k}}]. \tag{D2}$$

Next we carry out the calculation of the topological number in Eq. (D2) for the Hamiltonian Eq. (14) with the T_d symmetry. The chiral operator $C = \tau_1 \otimes R$ is diagonalized by the following matrix W ,

$$W = \frac{1}{\sqrt{2}} \begin{pmatrix} I_4 & iR \\ -iR & I_4 \end{pmatrix}, \tag{D3}$$

in which I_4 is the 4×4 identity matrix. The Hamiltonian $H_{\vec{k}}$ can be brought into a block off-diagonal form as

$$WH_{\vec{k}}W^\dagger = \begin{pmatrix} 0 & D_{\vec{k}} \\ D_{\vec{k}}^\dagger & 0 \end{pmatrix}, \quad (\text{D4})$$

in which

$$D_{\vec{k}} = H_L(\vec{k}) + \delta A(\vec{k}) - \mu + i\Delta_0(C_s + C_p A(\vec{k})). \quad (\text{D5})$$

Treating the inversion breaking term $\frac{\delta}{k_f} A(\vec{k})$ at the level of the first order degenerate perturbation theory, the band energies $\epsilon_{\pm}^{(1/2)}(\vec{k})$ and $\epsilon_{\pm}^{(3/2)}(\vec{k})$ of the spin-split light hole and heavy hole bands are given, respectively, by

$$\begin{aligned} \epsilon_{\pm}^{1/2}(\vec{k}) &= (2\lambda_2 + \lambda_1)k^2 \pm \delta|\Lambda^{(1/2)}(\vec{k})| - \mu, \\ \epsilon_{\pm}^{3/2}(\vec{k}) &= (2\lambda_2 - \lambda_1)k^2 \pm \delta|\Lambda^{(3/2)}(\vec{k})| - \mu. \end{aligned} \quad (\text{D6})$$

Up to the first order in $\delta/|\mu|$ and $\Delta_0/|\mu|$, the matrix $D_{\vec{k}}$ is diagonalized via a unitary transformation $U_{\vec{k}}$ as

$$D_{\vec{k}} = U_{\vec{k}} \text{diag}(\epsilon_{\nu}^{(\alpha)}(\vec{k}) + i\Delta_{\nu}^{(\alpha)}(\vec{k}))U_{\vec{k}}^\dagger, \quad (\text{D7})$$

in which $\alpha = \frac{3}{2}, \frac{1}{2}$, $\nu = \pm$, and $\Delta_{\nu}^{(\alpha)}(\vec{k}) = \Delta_0(C_s + \nu C_p |\vec{\Lambda}^{(\alpha)}(\vec{k})|)$. Then $Q_{\vec{k}}$ is derived as

$$Q_{\vec{k}} = U_{\vec{k}} \text{diag}(e^{i\theta_{\nu}^{(\alpha)}(\vec{k})})U_{\vec{k}}^\dagger, \quad (\text{D8})$$

in which $\tan \theta_{\nu}^{(\alpha)}(\vec{k}) = \Delta_{\nu}^{(\alpha)}(\vec{k})/\epsilon_{\nu}^{(\alpha)}(\vec{k})$. Plugging $Q_{\vec{k}}$ in Eq. (D2), we arrive at the topological index N_L as

$$N_L = \frac{1}{2\pi} \sum_{\alpha, \nu} \int_{\mathcal{L}} dk_l \partial_{k_l} \theta_{\nu}^{(\alpha)}(\vec{k}_l). \quad (\text{D9})$$

The bands of helicity $\pm \frac{1}{2}$ lie above the Fermi energy at the energy of the order of $|\mu|$, hence, they will not give rise to non-trivial contribution to N_L . For the bands of helicity $\pm 3/2$, the formula for N_L can be simplified to²⁴

$$N_L = -\frac{1}{2} \sum_{\nu} \sum_{\vec{k}_F} \text{sgn}(\partial_{k_l} \epsilon_{\nu}^{(3/2)}(\vec{k}_F)) \cdot \text{sgn}(\Delta_{\nu}^{(3/2)}(\vec{k}_F)), \quad (\text{D10})$$

where \vec{k}_F 's are the wavevectors at which the path \mathcal{L} crosses the Fermi surfaces. The equations $\epsilon_{\pm}^{(3/2)}(\vec{k}) = 0$ determines the smaller (larger) Fermi surface. These two Fermi surfaces touch along $[001]$ directions protected by the little group SD_{16} as analyzed in Sect. II C. Assuming $\Delta_s, \Delta_p > 0$, then the gap function $\Delta_{\pm}^{(3/2)}(\vec{k}_F)$ on the smaller Fermi surface are positive definite. A closed path \mathcal{L} always crosses the Fermi surface even times, and the sign of $(\partial_{k_l} \epsilon_{\nu}^{(3/2)}(\vec{k}_F))$ for crossing the Fermi surface from the inner to outer direction is opposite to that from the opposite directions, hence, the smaller Fermi surface

does not contribute the N_L as well. Then the formula is simplified to

$$N_L = -\frac{1}{2} \sum_{\vec{k}_F} \text{sgn}(\partial_{k_l} \epsilon_{-}^{(3/2)}(\vec{k}_F)) \cdot \text{sgn}(\Delta_{-}^{(3/2)}(\vec{k}_F)), \quad (\text{D11})$$

in which only the larger Fermi surface contributes.

For the Hamiltonian Eq. (14) with T_d symmetry, the sign of the pairing $\Delta_{-}^{(3/2)}(\vec{k}_F)$ inside the nodal loop is opposite to that outside the loop. Hence from Eq. (D11) the topological number for a closed path that encloses the nodal loop once is ± 1 , where the sign of N_L depends on the direction that the path is traversed.

The physical meaning of Eq. (D11) can be related to the sign structure of the gap functions along the incident and reflected wavevectors²⁴. Let \vec{k}_{\parallel} be an in-plane wavevector within the surface of interest. The infinite vertical line passing through \vec{k}_{\parallel} crosses the larger Fermi surface at two wavevectors with vertical components $k_{\perp 1}$ and $k_{\perp 2}$. Now we can enclose the infinite line with a semi-infinite circle and consider the topological number of the combined path \mathcal{L}_0 . From Eq. (D11), $N_{\mathcal{L}_0}$ is related to the sign difference between $\Delta_{-}^{(3/2)}(k_{\perp 1})$ and $\Delta_{-}^{(3/2)}(k_{\perp 2})$. On the other hand, $N_{\mathcal{L}_0}$ does not change by continuously deforming the path as long as the nodal circles are not touched. If after such a deformation no nodal loop is enclosed, the pairings of the incident and reflected wavevectors are of the same sign, corresponding to a topologically trivial situation. If two nodal loops are enclosed and the topological numbers from the two loops cancel, which is a topologically trivial situation again. In contrast, if only one nodal loop is enclosed, the topological number $N_{\mathcal{L}_0} = \pm 1$, for which the Majorana zero modes appear.

Appendix E: The method for solving surface states

In this appendix, the equation determining surface state is derived in the limit $\Delta_0 \ll \delta \ll |\mu|$. We first obtain the eight pairs of $\{\vec{k}_l, \Phi_l\}$ from Eq. (22) as functions of E_s , then plug them in $\det(\{\Phi_l\}_{1 \leq l \leq 8}) = 0$ to solve for E_s . The pairing strengths and the surface energy are parametrized as $\Delta_s = C_s \Delta_0$, $\Delta_p = C_p \Delta_0$ and $E_s = \epsilon \Delta_0$.

Due to the translation symmetry in xy -plane, (k_x, k_y) remain good quantum numbers. The momentum k_z solving Eq. (22) can be expanded as $k_z = \pm k_{0z} + \zeta \delta - i\xi \Delta_0$, in which k_{0z} is the magnitude of the z 'th component of the Fermi wavevector determined by the Luttinger-Kohn Hamiltonian, $\zeta \delta$ originates from the splitting of Fermi surfaces due to the inversion breaking term in the band structure, and $-i\xi \Delta_0$ is from the superconducting pairing. Denote $k_{0z}^{(3/2)}$ and $k_{0z}^{(1/2)}$ to be the above mentioned k_{0z} for the heavy and light hole bands, respectively. Since the Fermi energy crosses the heavy hole bands, $k_{0z}^{(3/2)}$ is

real, while $k_{0z}^{(1/2)}$ is purely imaginary. The expressions of $k_{0z}^{(3/2)}$ and $k_{0z}^{(1/2)}$ are

$$\begin{aligned} k_{0z}^{(3/2)} &= \sqrt{|\mu|/(2\lambda_2 - \lambda_1) - k_x^2 - k_y^2}, \\ k_{0z}^{(1/2)} &= -i\sqrt{|\mu|/(2\lambda_2 + \lambda_1) + k_x^2 + k_y^2}. \end{aligned} \quad (\text{E1})$$

We also denote $k_0^{(3/2)}$ and $k_0^{(1/2)}$ as

$$\begin{aligned} k_0^{(3/2)} &= \sqrt{|\mu|/(2\lambda_2 - \lambda_1)}, \\ k_0^{(1/2)} &= -i\sqrt{|\mu|/(2\lambda_2 + \lambda_1)}. \end{aligned} \quad (\text{E2})$$

We will discuss the heavy and light hole bands separately, and first consider the heavy hole bands. The superscript “3/2” on momentum will be dropped for simplicity. Denote \hat{a} to be the unit vector normal to the surface. Let $\vec{k}_{0\eta} = (k_x, k_y, \eta k_{0z})$ ($\eta = \pm 1$), and define $\mathcal{U}^{(3/2)}(\vec{k}_{0\eta})$ as

$$\mathcal{U}^{(3/2)}(\vec{k}_{0\eta}) = \begin{pmatrix} U(\hat{a}) & 0 \\ 0 & U(\hat{a})^{T,-1} \end{pmatrix} \begin{pmatrix} U(\hat{k}_{0\eta}) & 0 \\ 0 & U(\hat{k}_{0\eta})^{T,-1} \end{pmatrix}, \quad (\text{E3})$$

in which $U(\hat{a}) = e^{-iS_z\phi_a}e^{-iS_y\theta_a}$ and $U(\vec{k}_{0\eta}) = e^{-iS_z\phi_\eta}e^{-iS_y\theta_\eta}$, where θ_a and ϕ_a are the polar and azimuthal angles of \hat{a} , and θ_η and ϕ_η are those of the vector $\vec{k}_{0\eta}$. $\mathcal{U}^{(3/2)}(\vec{k}_{0\eta})$ corresponds to the helicity basis at momentum $\vec{k}_{0\eta}$. Plug $k_z = \eta k_{0z} + \zeta\delta - i\xi\Delta_0$ ($\eta = \pm 1$) into the Hamiltonian in Eq. (14), perform the transformation $\mathcal{U}^{(3/2)}(\vec{k}_{0\eta})^{-1}H(\vec{k})\mathcal{U}^{(3/2)}(\vec{k}_{0\eta})$, and project into the heavy hole bands. Then by keeping the leading order terms in the expansion over δ and Δ_0 , the H_L and H_A terms in Eq. (14) become

$$\begin{aligned} H'_L - \mu &= (\zeta\delta - i\xi\Delta_0)(2(\lambda_1 + \frac{5}{2}\lambda_2)\eta k_{0z} \\ &\quad - 2\lambda_2 k_0 P_{3/2}\{S_z, U(\vec{k}_{0\eta})^{-1}S_z U(\vec{k}_{0\eta})\}P_{3/2}), \\ H'_A &= \frac{\delta}{k_f} P_{3/2} U(\vec{k}_{0\eta})^{-1} U(\hat{a})^{-1} A(R_a \vec{k}_{0\eta}) \\ &\quad \cdot U(\hat{a}) U(\vec{k}_{0\eta}) P_{3/2}, \end{aligned} \quad (\text{E4})$$

in which $P_{3/2}$ is the projection operator to the heavy hole bands; the superscript of prime denotes the terms after the transformation and the projection; $\{, \}$ represents the anti-commutator of two matrices; and k_0 is $k_0^{(3/2)}$ with the superscript “3/2” omitted. H'_L and H'_A are 2×2 matrices after the projection to the heavy hole bands. H'_A is traceless, hence can be expanded in terms of Pauli matrices as

$$H'_A = \delta \vec{\Lambda}(\vec{k}_{0\eta}) \cdot \vec{\sigma}, \quad (\text{E5})$$

in which $\vec{\Lambda}(\vec{k}_{0\eta})$ is a three-component vector. Let $D(\vec{k}_{0\eta})$ be the transformation that diagonalizes H'_A . The eigenvalues of H'_A are $\pm\delta|\vec{\Lambda}(\vec{k}_{0\eta})|$, which leads to Fermi surface

splitting. The correction of the Fermi wave vector due to the splitting is given by $\zeta\delta$, and there are two values of ζ corresponding to the two eigenvalues of H'_A . In the following, for simplicity, we will term the basis after the transformation of $D(\vec{k}_{0\eta})$ as band structure basis.

Next we consider the effect of the superconducting pairing. Since $\Delta_0 \ll \delta$, as long as H'_A does not vanish, we can project the superconducting pairing onto the eigen-bases of the band Hamiltonian, and the corrections from the mixing between different spin-split bands are of higher orders in Δ_0/δ . Let P_ν ($\nu = \pm 1$) be the projection operator to one of the two band structure basis with eigenvalue $\nu\delta\sqrt{\vec{\Lambda}(\vec{k}_{0\eta})^2}$ of H'_A . Plug $k_z = \eta k_{0z} + \zeta\delta - i\xi\Delta_0$ into Eq. (22), and set k_z to be ηk_{0z} in the pairing Hamiltonian with corrections of high orders. Then Eq. (22) becomes a two-component eigen-equation, as

$$\begin{pmatrix} i\xi\gamma(\vec{k}_{0\eta}) - \epsilon & (-)^{\frac{1-\nu}{2}}\chi_\nu(\vec{k}_{0\eta}) \\ (-)^{\frac{1-\nu}{2}}\chi_\nu(\vec{k}_{0\eta})^* & -i\xi\gamma(\vec{k}_0) - \epsilon \end{pmatrix} \Phi' = 0, \quad (\text{E6})$$

in which

$$\begin{aligned} \gamma(\vec{k}_{0\eta}) &= -2(\lambda_1 + \frac{5}{2}\lambda_2)\eta k_{0z} + \\ &\quad 2\lambda_2 k_0 P_{3/2}\{S_z, U(\vec{k}_{0\eta})^{-1}S_z U(\vec{k}_{0\eta})\}P_{3/2}P_\nu, \\ \chi_\nu(\vec{k}_{0\eta}) &= P_\nu D(\vec{k}_{0\eta})^{-1}P_{3/2}U(\vec{k}_{0\eta})^{-1}U(\hat{a})^{-1}K(R_a \vec{k}_{0\eta}) \\ &\quad \cdot U(\hat{a})U(\vec{k}_{0\eta})P_{3/2}D(\vec{k}_{0\eta})P_\nu. \end{aligned} \quad (\text{E7})$$

The $\gamma(\vec{k}_{0\eta})$ term corresponds to the $O(\Delta_0)$ correction to the diagonal block in Eq. (22) from $-i\xi\Delta_0$ in $k_z = \eta k_{0z} + \zeta\delta - i\xi\Delta_0$, and the $\chi_\nu(\vec{k}_{0\eta})$ term is the projection to band structure basis of the superconducting pairing. The solutions of ξ and Φ' are given by

$$\begin{aligned} \xi^{(3/2)}(\vec{k}_{0\eta}; \nu) &= \sqrt{\frac{|\chi_\nu(\vec{k}_{0\eta})|^2 - \epsilon^2}{\gamma(\vec{k}_{0\eta})^2}}, \\ \Phi'^{(3/2)}(\vec{k}_{0\eta}; \nu) &= \begin{pmatrix} -(-)^{\frac{1-\nu}{2}}\chi_\nu(\vec{k}_{0\eta}) \\ i\xi(\vec{k}_{0\eta}, \nu)\gamma(\vec{k}_{0\eta}) - \epsilon \end{pmatrix}, \end{aligned} \quad (\text{E8})$$

in which ξ is chosen to be positive to match the boundary condition at $z \rightarrow -\infty$. The eigenvector Φ can be obtained from Φ' by performing the transformations $D(\vec{k}_{0\eta})$, $U(\vec{k}_{0\eta})$ and $U(\hat{a})$ back in sequence.

Now we turn to the light hole bands. Again the superscript “1/2” will be dropped in the following expressions for simplicity. The momentum in z -direction is in general $k_z = k_{0z} + \zeta\delta - i\xi\Delta_0$, where $k_{0z} = -i\sqrt{|\mu|/(2\lambda_2 + \lambda_1) + k_x^2 + k_y^2}$. $\text{Im}(k_{0z})$ is chosen to be negative so as to match the boundary condition at $z \rightarrow -\infty$. Let $\vec{k}_0 = (k_x, k_y, k_{0z})$, and define

$$U^{(1/2)}(\vec{k}_0) = \begin{pmatrix} U(\hat{a}) & 0 \\ 0 & U(\hat{a})^{T,-1} \end{pmatrix} \begin{pmatrix} U(\hat{k}_0) & 0 \\ 0 & U(\hat{k}_0)^{T,-1} \end{pmatrix}, \quad (\text{E9})$$

in which $U(\vec{k}_0) = e^{-iS_z\phi}e^{-iS_y\theta}$, where $\phi = \arctan(k_y/k_x)$ and $\theta = \arccos(k_{0z}/k_0)$. Unlike the heavy hole bands, here θ is purely imaginary since $|k_{0z}| > |k_0|$. Plug $k_z = k_{0z} + \zeta\delta - i\xi\Delta_0$ into the Hamiltonian in Eq. (14), perform the transformation $\mathcal{U}^{(1/2)}(\vec{k}_0)^{-1}H(\vec{k})\mathcal{U}^{(1/2)}(\vec{k}_0)$, and project into the light hole bands. Then by keeping the leading order terms in the expansion over δ and Δ_0 , the H_L and H_A terms become

$$\begin{aligned} H'_L - \mu &= (\zeta\delta - i\xi\Delta_0)(2(\lambda_1 + \frac{5}{2}\lambda_2)k_{0z} \\ &\quad - 2\lambda_2k_0P_{1/2}\{S_z, U(\vec{k}_0)^{-1}S_zU(\vec{k}_0)\}P_{1/2}), \\ H'_A &= \frac{\delta}{k_f}P_{1/2}U(\vec{k}_0)^{-1}U(\hat{a})^{-1}A(R_a\vec{k}_0) \\ &\quad \cdot U(\hat{a})U(\vec{k}_0)P_{1/2}, \end{aligned} \quad (\text{E10})$$

in which $P_{1/2}$ is the projection operator to the helicity $\pm 1/2$ bands, and the superscript of prime denotes the terms after the transformation and the projection. The eigenvalues of H'_A are $\pm\sqrt{\tilde{\Lambda}^2(\vec{k}_0)}$. H'_A introduces the correction of $\zeta\delta$ into the Fermi wave vectors. Let $D(\vec{k}_0)$ be the transformation that diagonalizes H'_A . It defines the band structure basis for the case of the light hole bands.

Let P_ν ($\nu = \pm 1$) be the projection operator to one of two band structure basis with eigenvalue $\nu\sqrt{\tilde{\Lambda}^2(\vec{k}_0)}$ of H'_A . For the treatment of the superconducting pairing, again by assuming $\Delta_0 \ll \delta$, the projection to the band structure basis can be performed, and the eigen-equation determining ξ and Φ is

$$\begin{pmatrix} i\xi\gamma(\vec{k}_0) - \epsilon & -(-)^{\frac{1-\nu}{2}}\chi_\nu(\vec{k}_0) \\ -(-)^{\frac{1-\nu}{2}}\tilde{\chi}_\nu(\vec{k}_0) & -i\xi\gamma(\vec{k}_0) - \epsilon \end{pmatrix} \Phi' = 0, \quad (\text{E11})$$

in which

$$\begin{aligned} \gamma(\vec{k}_0) &= -2(\lambda_1 + \frac{5}{2}\lambda_2)k_{0z} \\ &\quad + 2\lambda_2k_0P_\nu P_{1/2}\{S_z, U(\vec{k}_0)^{-1}S_zU(\vec{k}_0)\}P_{1/2}P_\nu, \\ \chi_\nu(\vec{k}_0) &= P_\nu D^{-1}(\vec{k}_0)P_{1/2}U(\vec{k}_0)^{-1}U(\hat{a})^{-1}K(R_a\vec{k}_0) \\ &\quad \cdot U(\hat{a})U(\vec{k}_0)P_{1/2}D(\vec{k}_0)P_\nu, \\ \tilde{\chi}_\nu(\vec{k}_0) &= P_\nu D^\dagger(\vec{k}_0)P_{1/2}U(\vec{k}_0)^\dagger U(\hat{a})^{-1}K(R_a\vec{k}_0^*) \\ &\quad \cdot U(\hat{a})U(\vec{k}_0)^\dagger P_{1/2}D(\vec{k}_0)^\dagger P_\nu. \end{aligned} \quad (\text{E12})$$

Then ξ and Φ' are solved as

$$\begin{aligned} \xi^{(1/2)}(\vec{k}_0; \nu, \iota) &= \iota \sqrt{\frac{\chi_\nu(\vec{k}_0)\tilde{\chi}_\nu^*(\vec{k}_0) - \epsilon^2}{\gamma(\vec{k}_0)^2}}, \\ \Phi'^{(1/2)}(\vec{k}_0; \nu, \iota) &= \begin{pmatrix} (-)^{(1-\nu)/2}\chi_\nu(\vec{k}_0) \\ i\xi(\vec{k}_0; \nu, \iota)\gamma(\vec{k}_0) - \epsilon \end{pmatrix}, \end{aligned} \quad (\text{E13})$$

in which $\iota = \pm 1$. The eigenvector Φ can be obtained from Φ' by performing the transformations $D(\vec{k}_0)$, $U(\vec{k}_0)$ and $U(\hat{a})$ back in sequence.

Plugging these expressions into the boundary condition at $z = 0$, we obtain the equation determining the energy of the surface states,

$$\det(\{\Phi^{(1/2)}(\vec{k}_0^{(1/2)}; \nu, \iota)\}_{\nu, \iota=\pm}, \{\Phi^{(3/2)}(\vec{k}_{0\eta}^{(1/2)}; \nu)\}_{\eta, \nu=\pm}) = 0, \quad (\text{E14})$$

in which

$$\begin{aligned} \Phi^{(1/2)}(\vec{k}_0^{(1/2)}; \nu, \iota) &= U^{(1/2)}(\vec{k}_0)\bar{D}^{(1/2)}(\vec{k}_0)\Phi'^{(1/2)}(\vec{k}_0; \nu, \iota), \\ \Phi^{(3/2)}(\vec{k}_{0\eta}^{(3/2)}; \nu) &= U^{(3/2)}(\vec{k}_{0\eta})\bar{D}^{(3/2)}(\vec{k}_{0\eta})\Phi'^{(3/2)}(\vec{k}_{0\eta}; \nu), \end{aligned} \quad (\text{E15})$$

where $\bar{D} = \text{diag}(D, D^{T,-1})$ is the extension of the matrix D to the particle-hole space. In Eq. (E15), all of the terms are in the 8-dimensional space. For those originally defined not to be 8-dimensional, we need to appropriately embed them into the 8-dimensional space. Eq. (E15) is the general equation for solving surface state energy, without restriction on the form of the inversion breaking term, nor on the form of the pairing Hamiltonian.

We further note that for the present case in which the Fermi energy only crosses the heavy hole bands, the 8×8 matrix in Eq. (E15) can be reduced to a 4×4 one when solving Majorana zero modes. The boundary condition requires that the eight vectors $\Phi_i^{(\alpha)}$ ($\alpha = 3/2, 1/2$, $1 \leq i \leq 4$) are linearly dependent. At zero energy, the four vectors $\Phi_i^{(1/2) \prime}$ in the light hole space in Eq. (E13) are linearly independent. Hence they must also be so at least in a neighborhood of $\epsilon = 0$. The vectors $\Phi_i^{(1/2)}$ are obtained from $\Phi_i^{(1/2) \prime}$ by the same transformation $D^{(1/2)}$. This means that $\Phi_i^{(1/2)}$ are also linearly independent in a neighborhood of $\epsilon = 0$. Thus the boundary condition can be simplified to $\det\{\mathcal{P}\Phi_i^{(3/2)}\}_{1 \leq i \leq 4} = 0$, where \mathcal{P} is the projection operator into the linear subspace orthogonal to the space spanned by $\{\Phi_i^{(1/2)}\}_{1 \leq i \leq 4}$.

Although the original boundary condition matrix in Eq. (E14) can be reduced to the heavy hole space, the light hole space cannot be neglected since they touch with the heavy hole bands at the Γ point. If the two sets of bands are separated by a band gap E_g much greater than the value of the chemical potential, then the light hole bands are inert up to leading order of $|\mu|/E_g$. In the current situation, they enter into the reduced 4×4 boundary condition matrix, which is a reflection of the spin-3/2 nature of the system.

Appendix F: Symmetry properties in QPI patterns

We discuss in this section the implications of particle-hole, TR, chiral and C_{3v} symmetries on the QPI patterns for (111)-surface.

1. Particle-hole symmetry

In this part, we discuss the consequence of particle-hole symmetry in QPI patterns.

First consider the non-magnetic impurity. Let P_{sf} be the projection operator to the subspace of the surface states. In Born approximation and only taking into account the contribution from Majorana zero modes, $\Delta\rho^{(00)}(\omega, \vec{r})$ can be expressed as

$$\begin{aligned}\Delta\rho^{(00)}(\omega, \vec{r}) &= -\frac{1}{2\pi}\text{ImTr}[(1+\tau_3)\langle\vec{r}|P_{sf}\frac{1}{\omega-H+i\epsilon} \\ &\quad P_{sf}H_{\text{imp}}P_{sf}\frac{1}{\omega-H+i\epsilon}P_{sf}|\vec{r}\rangle], \\ &= -\frac{1}{2\pi}\text{Im}[(\frac{1}{\omega+i\epsilon})^2\text{Tr}((1+\tau_3) \\ &\quad \langle\vec{r}|P_{sf}V_{\text{imp}}P_{sf}|\vec{r}\rangle)],\end{aligned}\quad (\text{F1})$$

in which V_{imp} is a scalar potential. Particle-hole symmetry leads to

$$\langle\vec{r}|P_{sf}H_{\text{imp}}P_{sf}|\vec{r}\rangle = -\tau_1\langle\vec{r}|P_{sf}V_{\text{imp}}P_{sf}|\vec{r}\rangle^*\tau_1. \quad (\text{F2})$$

Since $\langle\vec{r}|P_{sf}H_{\text{imp}}P_{sf}|\vec{r}\rangle$ is hermitian, $\text{Tr}\langle\vec{r}|P_{sf}H_{\text{imp}}P_{sf}|\vec{r}\rangle$ vanishes due to Eq. (F2). Thus

$$\Delta\rho^{(00)}(\omega, \vec{r}) = -\frac{1}{2\pi}\text{Im}(\frac{1}{\omega+i\epsilon})^2\text{Tr}[\tau_3\langle\vec{r}|P_{sf}H_{\text{imp}}P_{sf}|\vec{r}\rangle]. \quad (\text{F3})$$

Next consider the magnetic impurity. In the same approximations, we have

$$\begin{aligned}\Delta\rho^{ij}(\omega, \vec{r}) &= -\frac{1}{2\pi}\text{ImTr}[(\frac{1}{\omega+i\epsilon})^2(1+\tau_3) \\ &\quad \Sigma^i\langle\vec{r}|P_{sf}\Sigma^jV_{\text{imp}}P_{sf}|\vec{r}\rangle].\end{aligned}\quad (\text{F4})$$

Particle-hole symmetry implies that

$$\langle\vec{r}|P_{sf}\Sigma^jH_{\text{imp}}P_{sf}|\vec{r}\rangle = -\tau_1\langle\vec{r}|P_{sf}\Sigma^jH_{\text{imp}}P_{sf}|\vec{r}\rangle^*\tau_1. \quad (\text{F5})$$

Combining with $\tau_1\Sigma^i\tau_1 = -\Sigma^{i*}$, we obtain $\text{Tr}(\tau_3\Sigma^i\langle\vec{r}|P_{sf}\Sigma^jV_{\text{imp}}P_{sf}|\vec{r}\rangle) = 0$, and

$$\begin{aligned}\Delta\rho^{ij}(\omega, \vec{r}) &= -\frac{1}{2\pi}\text{Im}[(\frac{1}{\omega+i\epsilon})^2 \\ &\quad \text{Tr}(\Sigma^i\langle\vec{r}|P_{sf}\Sigma^jV_{\text{imp}}P_{sf}|\vec{r}\rangle)].\end{aligned}\quad (\text{F6})$$

2. Time reversal symmetry

In addition to the suppression of scatterings between TR related Majorana islands, TR symmetry also requires that $\Delta\rho^{\mu 0} = 0$, and $\Delta\rho^{0\nu} = 0$ in Born approximation, where $\mu, \nu \neq 0$. We show these properties in this part.

It can be proved that in Born approximation, TR symmetry leads to

$$\begin{aligned}\Delta\rho^{\mu\nu}(\omega, \vec{r}) &= -\frac{1}{2\pi}\text{ImTr}\langle\vec{r}|(1+\tau_3)(T^{-1}\Sigma^\mu T) \\ &\quad \cdot V_{\text{imp}}(T^{-1}\Sigma^\nu T)\frac{1}{\omega-H+i\epsilon}|\vec{r}\rangle.\end{aligned}\quad (\text{F7})$$

Since Σ^0 is invariant under TR operation and Σ^i ($i = 1, 2, 3$) changes sign under TR operation, it is clear that $\Delta\rho^{\mu\nu}$ vanishes when $\mu = 0, \nu \neq 0$ or $\mu \neq 0, \nu = 0$.

3. Chiral symmetry

TR operation reverses the sign of Σ^ν when $\nu = 1, 2, 3$, and keeps it invariant when $\nu = 0$. Particle-hole operation reverses the sign of Σ_ν for all $\nu = 0, 1, 2, 3$. Chiral operation is the composition of TR and particle-hole operations. Hence the selection rule of chiral symmetry is that H_{imp}^ν couples Majorana islands with opposite chiral indices when $\nu = 0$, and those with the same chiral index when $\nu = 1, 2, 3$.

4. C_{3v} symmetry

The little group of the (111)-surface within the T_d group is C_{3v} . In this part, we analyze the consequence of C_{3v} symmetry on the QPI patterns in Born approximation. Since $\Delta\rho_{sf}^{00}(\omega, \vec{q})$ is invariant under C_{3v} , and $\Delta\rho_{sf}^{\mu\nu}(\omega, \vec{q}) = 0$ if one of $\{\mu, \nu\}$ is zero, here we consider $\mu, \nu \neq 0$.

In Born approximation

$$\begin{aligned}\Delta\rho^{\mu\nu}(\omega, \vec{r}) &= -\frac{1}{2\pi}\text{ImTr}[(1+\tau_3)\Sigma^\mu\langle\vec{r}| \\ &\quad V_{\text{imp}}(\vec{r})\Sigma^\nu\frac{1}{\omega-H+i\epsilon}|\vec{r}\rangle].\end{aligned}\quad (\text{F8})$$

Since C_{3v} is the symmetry group of the system, for $\mathcal{C} \in C_{3v}$, $\Delta\rho^{\mu\nu}(\omega, \vec{r})$ can also be written as

$$\begin{aligned}\Delta\rho^{\mu\nu}(\omega, \vec{r}) &= -\frac{1}{2\pi}\text{ImTr}[(1+\tau_3)\mathcal{C}\Sigma^\mu\mathcal{C}^{-1}\langle C\vec{r}| \\ &\quad \cdot V_{\text{imp}}(\vec{r})\mathcal{C}\Sigma^\nu\mathcal{C}^{-1}\frac{1}{\omega-H+i\epsilon}|C\vec{r}\rangle],\end{aligned}\quad (\text{F9})$$

in which \mathcal{C} is the corresponding 3×3 rotation matrix. Using $\mathcal{C}\Sigma^\mu\mathcal{C}^{-1} = \Sigma^\alpha C_{\alpha\mu}$, $\Delta\rho^{\mu\nu}(\omega, \vec{r})$ satisfies

$$\Delta\rho^{\mu\nu}(\omega, \vec{r}) = \Delta\rho^{\alpha\beta}(\omega, C\vec{r})C_{\alpha\mu}C_{\beta\nu}, \quad (\text{F10})$$

for any $\mathcal{C} \in C_{3v}$.

For fixed ω, \vec{q} , define $\Delta\rho_{sf}(\omega, \vec{q})$ as the 3×3 matrix whose $\mu\nu$ element is $\Delta\rho_{sf}^{\mu\nu}(\omega, \vec{q})$. The above analysis shows that

$$\Delta\rho_{sf}(\omega, C\vec{q}) = C\Delta\rho_{sf}(\omega, \vec{q})C^T, \quad (\text{F11})$$

for any $C \in C_{3v}$. This is the relation that $\Delta\rho_{sf}(\omega, \vec{q})$ must satisfy due to the C_{3v} symmetry.

-
- ¹ X.-L. Qi and S.-C. Zhang, Rev. Mod. Phys. **83**, 1057 (2011).
 - ² G. E. Volovik, *The universe in a helium droplet* (Oxford University Press, 2003).
 - ³ A. J. Leggett, Rev. Mod. Phys. **47**, 331 (1975).
 - ⁴ G. E. Volovik, J. Exp. Theor. Lett. **70**, 609 (1999).
 - ⁵ N. Read and D. Green, Phys. Rev. B **61**, 10267 (2000).
 - ⁶ A. Y. Kitaev, Phys. Uspekhi **44**, 1 (2001).
 - ⁷ X.-L. Qi, T. L. Hughes, S. Raghu, and S.-C. Zhang, Phys. Rev. Lett. **102**, 187001 (2009).
 - ⁸ D. A. Ivanov, Phys. Rev. Lett. **86**, 268 (2001).
 - ⁹ J. Alicea, Y. Oreg, G. Refael, F. von Oppen, and M. P. A. Fisher, Nat. Phys. **7**, 412 (2011).
 - ¹⁰ J. C. Y. Teo and C. L. Kane, Phys. Rev. Lett. **104**, 046401 (2010).
 - ¹¹ A. P. Schnyder, S. Ryu, A. Furusaki, and A. W. W. Ludwig, Phys. Rev. B **78**, 195125 (2008).
 - ¹² A. Kitaev, V. Lebedev, and M. Feigel'man, in AIP Conf. Proc. (AIP, 2009), pp. 22-30.
 - ¹³ S. Ryu, A. P. Schnyder, A. Furusaki, and A. W. W. Ludwig, New J. Phys. **12** (2010).
 - ¹⁴ R. Balian and N. R. Werthamer, Phys. Rev. **131**, 1553 (1963).
 - ¹⁵ S. B. Chung and S.-C. Zhang, Phys. Rev. Lett. **103**, 235301 (2009).
 - ¹⁶ Y.-M. Lu, T. Xiang, and D.-H. Lee, Nat. Phys. **10**, 1, (2014).
 - ¹⁷ C.-R. Hu, Phys. Rev. Lett. **72**, 1526 (1994).
 - ¹⁸ G. E. Volovik, in *Exotic Properties of Superfluid ^3He* (WORLD SCIENTIFIC, 1992).
 - ¹⁹ C. Wu and J. E. Hirsch, Phys. Rev. B **81**, 020508 (2010).
 - ²⁰ Y. Li and C. Wu, Sci. Rep. **2**, 392 (2012).
 - ²¹ Y. Li and F. D. M. Haldane, ArXiv:1510.01730 (2015).
 - ²² C.-K. Chiu, J. C. Teo, A. P. Schnyder, and S. Ryu, Rev. Mod. Phys. **88**, 035005 (2016).
 - ²³ T. Mizushima, Y. Tsutsumi, T. Kawakami, M. Sato, M. Ichioka, and K. Machida, J. Phys. Soc. Japan **85**, 022001 (2016).
 - ²⁴ A. P. Schnyder, P. M. R. Brydon, and C. Timm, Phys. Rev. B **85**, 024522 (2012).
 - ²⁵ A. P. Schnyder and P. M. R. Brydon, J. Phys. Condens. Matter **27**, 243201 (2015).
 - ²⁶ A. P. Schnyder and S. Ryu, Phys. Rev. B - Condens. Matter Mater. Phys. **84**, 060504 (2011).
 - ²⁷ P. M. R. Brydon, A. P. Schnyder, and C. Timm, Phys. Rev. B **84**, 020501 (2011).
 - ²⁸ M. Smidman, M. B. Salamon, H. Q. Yuan, and D. F. Agterberg (2016).
 - ²⁹ M. Sato, Y. Tanaka, K. Yada, and T. Yokoyama, Phys. Rev. B **83**, 224511 (2011).
 - ³⁰ S. Kashiwaya and Y. Tanaka, Reports on Progress in Physics **63**, 1641 (2000).
 - ³¹ Y. Tanaka, Y. Mizuno, T. Yokoyama, K. Yada, and M. Sato, Phys. Rev. Lett. **105**, 097002 (2010).
 - ³² J. S. Hofmann, R. Queiroz, and A. P. Schnyder, Phys. Rev. B **88**, 134505 (2013).
 - ³³ Y. Li, D. Wang, and C. Wu, New J. Phys. **15**, 085002 (2013).
 - ³⁴ A. C. Potter and P. A. Lee, Phys. Rev. Lett. **112**, 117002 (2014).
 - ³⁵ Carsten Timm, Stefan Rex, and P. M. R. Brydon, Phys. Rev. B **91**, 180503 (2015).
 - ³⁶ T.-L. Ho and S. Yip, Phys. Rev. Lett. **82**, 247 (1999).
 - ³⁷ C. Wu, J.-P. Hu, and S.-C. Zhang, Phys. Rev. Lett. **91**, 186402 (2003).
 - ³⁸ C. Wu, Mod. Phys. Lett. B **20**, 1707 (2006).
 - ³⁹ C. Wu, J.-P. Hu, and S.-C. Zang, Int. J. Mod. Phys. B **24**, 311 (2010).
 - ⁴⁰ W. Yang, Y. Li, and C. Wu, Phys. Rev. Lett. **117**, 075301 (2016).
 - ⁴¹ C. Fang, B. A. Bernevig, and M. J. Gilbert, Phys. Rev. B **91**, 165421 (2015).
 - ⁴² S. A. A. Ghorashi, S. Davis, and M. S. Foster, Phys. Rev. B **95**, 144503 (2017).
 - ⁴³ Z. K. Liu, L. X. Yang, S.-C. Wu, C. Shekhar, J. Jiang, H. F. Yang, Y. Zhang, S. K. Mo, Z. Hussain, B. Yan, C. Felser, and Y. L. Chen, Nat. Commun. **7**, 12924 (2016).
 - ⁴⁴ H. Kim *et al.*, ArXiv:1603.03375, (2016).
 - ⁴⁵ P. Brydon, L. Wang, M. Weinert, and D. Agterberg, Phys. Rev. Lett. **116**, 177001 (2016).
 - ⁴⁶ J. Yang and Z.-X. Liu, ArXiv:1605.05805 (2016).
 - ⁴⁷ S. Chadov, X. Qi, J. Kübler, G. H. Fecher, C. Felser, and S.-C. Zhang, Nat. Mater. **9**, 541 (2010).
 - ⁴⁸ H. Lin, L. A. Wray, Y. Xia, S. Xu, S. Jia, R. J. Cava, A. Bansil, and M. Z. Hasan, Nat. Mater. **9**, 546 (2010).
 - ⁴⁹ N. P. Butch, P. Syers, K. Kirshenbaum, A. P. Hope, and J. Paglione, Phys. Rev. B **84**, 220504 (2011).
 - ⁵⁰ P. A. Frigeri, D. F. Agterberg, A. Koga, and M. Sigrist, Phys. Rev. Lett. **92**, 097001 (2004).
 - ⁵¹ Q.-H. Wang and D.-H. Lee, Phys. Rev. B **67**, 020511 (2003).
 - ⁵² W.-C. Lee and C. Wu, Phys. Rev. Lett. **103**, 176101 (2009).
 - ⁵³ W.-C. Lee, C. Wu, D. P. Arovas, and S.-C. Zhang, Phys. Rev. B **80**, 245439 (2009).
 - ⁵⁴ S. Kourtis, J. Li, Z. Wang, A. Yazdani, and B. A. Bernevig, Phys. Rev. B **93**, 041109 (2016).
 - ⁵⁵ L. Yu, Acta Phys. Sin. **21**, 75 (1965).
 - ⁵⁶ H. Shiba, Prog. Theor. Phys. **40**, 435 (1968).
 - ⁵⁷ A. V. Balatsky, I. Vekhter, and Jian-Xin Zhu, Rev. Mod. Phys. **78**, 373 (2006).
 - ⁵⁸ C. Timm, A. P. Schnyder, D. F. Agterberg, and P. M. R. Brydon, ArXiv:1707.02739 (2017).
 - ⁵⁹ I. Boettcher and I. F. Herbut, ArXiv:1707.03444 (2017).
 - ⁶⁰ L. Savary, J. Ruhman, J. W. F. Venderbos, L. Fu, and P. A. Lee, ArXiv:1707.03831 (2017).